WILEY JCN RESEARCH IN SYSTEMS NEUROLOGY · THE JOURNAL OF COMPARATIVE NEUROLOGY

RESEARCH ARTICLE

Matrix-free mass spectrometry imaging of mouse brain tissue sections on silicon nanopost arrays

Jarod A. Fincher[1] | **Jacqueline E. Dyer[1]** | **Andrew R. Korte[1]** | **Sridevi Yadavilli[2]** | **Nicholas J. Morris[3]** | **Akos Vertes[1]**

[1]George Washington University, Washington, District of Columbia 20052

[2]Research Center for Genetic Medicine, Children's National Medical Center, Washington, District of Columbia 20010

[3]UES, Inc., Beavercreek, Ohio 45432

Correspondence
Akos Vertes, Department of Chemistry, George Washington University, 800 22nd Street, N.W., Washington, DC 20052.
Email: vertes@gwu.edu

Mass spectrometry imaging (MSI) is capable of detection and identification of diverse classes of compounds in brain tissue sections, whereas simultaneously mapping their spatial distributions. Given the vast array of chemical components present in neurological systems, as well as the innate diversity within molecular classes, MSI platforms capable of detecting a wide array of species are useful for achieving a more comprehensive understanding of their biological roles and significance. Currently, matrix-assisted laser desorption ionization (MALDI) is the method of choice for the molecular imaging of brain samples by mass spectrometry. However, nanostructured laser desorption ionization platforms, such as silicon nanopost arrays (NAPA), are emerging as alternative MSI techniques that can provide complementary insight into molecular distributions in the central nervous system. In this work, the molecular coverage of mouse brain lipids afforded by NAPA-MSI is compared to that of MALDI-MSI using two common MALDI matrices. In positive ion mode, MALDI spectra were dominated by phosphatidylcholines and phosphatidic acids. NAPA favored the ionization of phosphatidylethanolamines and glycosylated ceramides, which were poorly detected in MALDI-MSI. In negative ion mode, MALDI favored sulfatides and free fatty acids, whereas NAPA spectra were dominated by signal from phosphatidylethanolamines. The complementarity in lipid coverages between the NAPA- and MALDI-MSI platforms presents the possibility of selective lipid analysis and imaging dependent upon which platform is used. Nanofabrication of the NAPA platform offers better uniformity compared to MALDI, and the wider dynamic range offered by NAPA promises improved quantitation in imaging.

KEYWORDS

brain, laser desorption ionization, lipidomics, MALDI, mass spectrometry imaging, nanopost arrays, RRID:SCR_003817, RRID:SCR_004633, RRID:SCR_007712, RRID:SCR_010500, RRID:SCR_012040

1 | INTRODUCTION

The ability to capture and visualize spatial distributions of biomolecules such as proteins, peptides, lipids, and metabolites within biological systems is fundamental to furthering their understanding and drive advances in fields such as medical diagnostics (Neubert & Walch, 2013; Schubert, Weiland, Baune, & Hoffmann, 2016). Recent technological advancements in instrumentation and software have made mass spectrometry imaging (MSI), an analytical technique capable of

detecting and characterizing a wide variety of molecular species while simultaneously mapping their spatial distributions, a viable and promising tool for this purpose. MSI platforms have undergone rapid development, and MSI now offers the possibility of providing detailed chemical information down to subcellular spatial resolutions (Zavalin et al., 2012). This ability of simultaneously gathering chemical and spatial information from precise coordinates along a biological tissue section is helping applications of MSI in fields such as the pharmaceutical industry and clinical diagnostics (Buchberger, DeLaney,

Johnson, & Li, 2018; Gowda et al., 2008). MSI is now being applied in fields such as neurology and neuropsychopharmacology, helping provide insight into debilitating neurological diseases, such as Parkinson's and Alzheimer's, as well as traumatic brain injuries (Braidy et al., 2014; Shariatgorji, Svenningsson, & Andren, 2014; Woods et al., 2013). Given that more than half of the dry weight of the human brain consists of lipids, and the role lipids play in signaling pathways, their importance in neurological disease states is under investigation (Di Paolo & Kim, 2011).

Secondary ion mass spectrometry (SIMS) and matrix-assisted laser desorption ionization-mass spectrometry (MALDI-MS) are the most extensively studied and broadly used MSI platforms. In a typical SIMS experiment, a focused primary ion beam is rastered across a tissue surface, imparting enough energy into the surface to cause desorption and formation of secondary ions. Among many other applications, this technique has demonstrated successful imaging of lipids in mouse brain tissue, as well as drugs used to treat neurological disorders (Sjovall, Lausmaa, & Johansson, 2004; Todd, Schaaff, Chaurand, & Caprioli, 2001; Touboul et al., 2004). In a MALDI-MS experiment, a UV-absorbing matrix is deposited onto a sample, such as a tissue section. A laser is then rastered over the sample surface and absorption of incident laser light by the matrix leads to desorption and ionization of the material within the sample. These ions are then analyzed by the mass spectrometer (Caprioli, Farmer, & Gile, 1997). This method has led to remarkably successful detection and imaging of proteins, peptides, lipids, and metabolites from biological tissues (Hutchinson et al., 2005; Jackson et al., 2007; Kertesz et al., 2008; Miura et al., 2010; Seeley, Oppenheimer, Mi, Chaurand, & Caprioli, 2008). The broad detection capabilities offered by MALDI-MSI can be attributed to the array of possible matrix choices, with many matrices favoring ionization of certain molecules or molecular classes.

While MALDI has irrefutably laid the foundation for MSI, it has also suffered from inherent limitations. For example, the requirement of matrix deposition for efficient ionization of analytes can lead to undesirable effects such as analyte diffusion and inhomogeneous crystal formation (Baluya, Garrett, & Yost, 2007; Goodwin, 2012; Thomas, Charbonneau, Fournaise, & Chaurand, 2012). Both of these issues can contribute to a reduction in achievable spatial resolution, arguably the most important parameter in MSI. Inhomogeneous crystallization in particular can lead to the creation of "hot-spots," so that apparent ion distributions are not representative of their natural distributions (Alexandrov, 2012). Lastly, vacuum stability is a concern for some MALDI matrices. Given the generally long acquisition times required for MSI experiments, sublimation (and possibly redeposition) of matrix in the vacuum of the MALDI source can lead to contamination of the source, loss of signal, and inaccurate apparent molecular distributions (Potocnik, Porta, Becker, Heeren, & Ellis, 2015).

Several matrix-free ionization platforms, including desorption/ionization on silicon, nanostructure-initiator mass spectrometry, and some ambient ionization approaches, such as desorption electrospray ionization and laser ablation electrospray ionization, have been developed in an effort to overcome these issues and reduce the sample preparation requirements (Nemes & Vertes, 2007; Northen et al., 2007; Shen et al., 2001; Takats, Wiseman, Gologan, & Cooks, 2004; Wei, Buriak, & Siuzdak, 1999). Furthermore, these matrix-free

ionization platforms were used to successfully image spatial distributions of metabolites and lipids in mouse brain tissue sections (Greving, Patti, & Siuzdak, 2011; Nemes, Woods, & Vertes, 2010; Wiseman, Ifa, Song, & Cooks, 2006; Yanes et al., 2009). Among these, laser desorption ionization (LDI) from a silicon nanopost array (NAPA) has emerged as a promising matrix-free LDI platform that offers broad molecular coverage, ultratrace sensitivity, and tissue imaging capabilities (Korte, Stopka, Morris, Razunguzwa, & Vertes, 2016; Stopka et al., 2016; Walker, Stolee, Pickel, Retterer, & Vertes, 2010; Walker, Stolee, & Vertes, 2012). Furthermore, thanks to advancements in photolithography, these NAPAs can be structurally modified and tuned to provide localized electric field enhancements, producing higher ion yields, whereas simultaneously requiring lower laser fluences (Morris et al., 2015; Stopka et al., 2018).

In this work, we compare the abilities of NAPA-MS and MALDI-MS with two common matrices to ionize and image various lipid classes from pure standards and mouse brain tissue sections. To characterize the differences in ionization efficiencies, relative quantitation was used to compare the lipid signal from standards and from the complex matrix of mouse brain tissue.

2 | MATERIALS AND METHODS

2.1 | Chemicals

LC-MS grade solvents methanol (MeOH; catalog no. A452-4), chloroform (catalog no. C6704-4), isopropyl alcohol (IPA; catalog no. A461-4), acetonitrile (catalog no. A955-4), and water (catalog no. W6-212) were purchased from Fisher Scientific (Hampton, NH). Lipid standards 1,2-dielaidoyl-sn-glycero-3-phosphocholine (PC; catalog no. 850376), 1-(1Z-octadecenyl)-2-docosahexaenoyl-sn-glycero-3-phosphoethanolamine (PEp; catalog no. 852806), 1-stearoyl-2-arachidonoyl-sn-glycero-3-phosphoethanolamine (PE; catalog no. 850804), N-stearoyl-D-erythro-sphingosylphosphorylcholine (SM; catalog no. 860586), 3-O-sulfo-D-galactosyl-ß1-1′-N-nervonoyl-D-erythro-sphingosine (ST; catalog no. 860571), D-galactosyl-ß1-1′-N-[2″(R)-hydroxystearoyl]-D-erythro-sphingosine (HexCer; catalog no. 860840) were purchased from Avanti Polar Lipids, Inc. (Alabaster, AL). 2,5-Dihydroxybenzoic acid (DHB; catalog no. 58707) and 9-aminoacridine (9-AA; catalog no. 92817) and carboxymethylcellulose (CMC; catalog no. C4888) were purchased from Sigma-Aldrich (St. Louis, MO).

2.2 | Fabrication of NAPA imaging chips

The fabrication of silicon nanoposts have been described elsewhere (Korte et al., 2016). Briefly, silicon nanoposts are fabricated from low resistivity (0.001–0.005 Ω cm) ⟨100⟩ p-type silicon wafers (Silicon Valley Microelectronics, Inc., Santa Clara, CA) using deep ultraviolet projection photolithography and deep reactive ion etching. The fabricated wafers are covered by nanoposts with dimensions of 1,100 nm in height, 150 nm in diameter, and a periodicity of 337 nm. The wafers are then diced into 20 mm squares and ready for tissue imaging experiments.

2.3 | Preparation of lipid standards

For MALDI analysis, lipid standards (HexCer, PC, PE, PEp, SM, and ST) were prepared as a mixture at 0.1 mg/ml each in 2:8:1 MeOH:IPA:H_2O. The matrices DHB and 9-AA were chosen for comparison to NAPA based on their frequent use for MALDI analysis in positive and negative ion modes, respectively. Matrices DHB and 9-AA were separately dissolved in aliquots of the lipid standard solutions at 10 mg/ml. A volume of 1 μl of each of the matrix-standard mixtures were directly pipetted onto a stainless steel MALDI plate and allowed to dry under atmosphere. For NAPA analysis, the same lipid standards were prepared as a mixture at 0.1 mg/ml each in chloroform. Five hundred nanoliter volumes were directly pipetted onto NAPA chips. All analyses were performed in triplicates.

2.4 | Tissue prep for MSI

Whole mouse (Jackson Laboratory, Bar Harbor, ME, RRID: SCR_004633) brains were provided by Children's National Medical Center (Washington, DC) in accordance with the approval of Institutional Animal Care and Use Committee. Immediately after removal, mouse brains were flash-frozen in liquid nitrogen and stored at −80 °C. Prior to analysis, mouse brains were removed from the −80 °C freezer, submerged in 2.5% aqueous CMC embedding medium, and placed into a −22 °C cryomicrotome (CM1800, Leica Microsystems Inc., Nussloch, Germany) for ~30 min to allow the embedding medium to solidify and the tissue to reach thermal equilibrium. Serial coronal sections were cut with a 10 μm thickness and thaw-mounted onto NAPA imaging chips and Superfrost Plus microscope slides (12–550-15, Fisher Scientific, Hampton, NH) for NAPA-LDI-MSI and MALDI-MSI experiments, respectively. Mounted tissue sections were then dried in a vacuum desiccator for 30 min.

For matrix deposition in MALDI-MSI experiments, an airbrush (TS-100D, Paasche, Chicago, IL) was used to spray 100 mg/ml DHB in 60% MeOH and 12.5 mg/ml 9-AA in 90% MeOH in positive and negative ion mode operation, respectively. For uniform coverage, 10–15 cycles consisting of 10 s spraying followed by 30 s drying were used for DHB deposition, whereas as 25–30 cycles were used for 9-AA.

2.5 | Imaging data acquisition and processing

A MALDI-LTQ-Orbitrap XL mass spectrometer (Thermo Scientific, San Jose, CA) was used to acquire all MS and MSI data. Silicon NAPA imaging chips containing tissue sections were secured to a MALDI stainless steel plate using double-sided carbon tape (Ted Pella, Inc., Redding, CA), and inserted into the instrument. All tissue sections were registered by the instrument using the tissue imaging function. The laser spot size at the sample surface was ~100 × 80 μm and a raster step size of 100 μm was used throughout. To improve sensitivity, ions from multiple laser shots were collected in the ion trap before they were transferred to the orbitrap analyzer. All tissue imaging experiments were performed at a laser fluence of 120 mJ/cm^2, with 3 laser shots per orbitrap scan for NAPA-LDI-MSI and 10 shots/scan for MALDI-MSI. For experiments with lipid standards, a laser fluence of 48 mJ/cm^2 and 3 laser shots/scan were used for NAPA-MS

analysis, whereas a laser fluence of 16 mJ/cm^2 and 5 laser shots/scan were used for MALDI-MS analysis. Mass spectra for standard analysis and tissue imaging were acquired in the orbitrap mass analyzer between m/z 180 and 1,000 with a resolving power setting of 30,000. A nitrogen laser, emitting radiation at 337 nm and an angle of 32° to the normal with a repetition rate of 60 Hz, was used to desorb and ionize the lipid standards and mouse brain tissue sections. The MSI experiments on tissue sections, with areas of ~8 × 15 mm^2, required an average scan time of ~2.5 hr.

All raw data files (*.raw) were imported into ImageQuest (Thermo Scientific, San Jose, CA) for processing and generation of chemical images with mass tolerance of ≤5 mDa. Spectra from regions of interest within the tissue were extracted and imported into mMass for peak picking and deisotoping (Strohalm, Kavan, Novak, Volny, & Havlicek, 2010). The corresponding m/z values were compared against an in-house reference list constructed from the Metlin (https://metlin.scripps.edu, RRID:SCR_010500), LipidMaps (http://www.lipidmaps.org/, RRID:SCR_003817), and HMDB (http://www.hmdb.ca/, RRID:SCR_007712) databases.

2.6 | Tissue extraction and UPLC-MS/MS

Brain lipid extracts were prepared by placing intact mouse brain into a 5 ml centrifuge tube containing 2 ml of 70% methanol (chilled to −80 °C) and disrupting it using a hand-held homogenizer (TissueRuptor II, Qiagen, Hilden, Germany). After homogenization, 2 ml of chloroform was added to yield distinct aqueous and organic phases. The sample was then briefly vortexed and centrifuged for 10 min at 14,000×g and 4 °C. Approximately 2.5 ml of the organic phase was removed and aliquoted to five separate tubes. The extract aliquots were then dried under vacuum and stored at −80 °C until analysis.

To aid in the identification of lipids detected in MSI experiments, a UPLC system (Acquity, Waters, Milford, MA) was interfaced to the MALDI-LTQ-Orbitrap XL mass spectrometer (Thermo Scientific, San Jose, CA). Chromatographic separation was performed on a Waters Acquity UPLC CSH C18 column (2.1 × 100 mm, 1.7 μm) at 55 °C with a flow rate of 400 μl min^{-1}. Mobile phase A composition was 60:40 acetonitrile:water with 10 mM ammonium formate and 0.1% formic acid. Mobile phase B composition was 90:10 isopropanol:acetonitrile with 10 mM ammonium formate and 0.1% formic acid. Gradient flow conditions were as follows: 0 min 60% A, 2.0 min 57% A, 2.1 min 50% A, 12.0 min 46% A, 12.1 min 30% A, 18.0 min 1% A, 18.1–20.0 min 60% A.

Mass spectra were acquired from the m/z 150–1,800 region in the orbitrap mass analyzer with a resolving power setting of 30,000. Tandem MS spectra were acquired in a data dependent fashion by selecting the most intense ion between m/z 350–1,000 in the MS master scan. After MS/MS acquisition, ions were excluded from selection for 10 s. Selected precursor ions were isolated with an m/z window of ±1 and fragmented using higher-energy collisional induced dissociation with a normalized collision energy of 25.

UPLC-MS/MS data were processed using MSconvert and mzMINE (version 2.23, RRID:SCR_012040) before being imported into LipidMatch for identification (Koelmel et al., 2017). Lipid

identifications were accepted for compounds which exhibited a precursor ion *m/z* error ≤10 mDa and tandem MS peaks corresponding to matching fatty acid chain lengths.

3 | RESULTS

To assess the ionization efficiencies for both NAPA- and MALDI-MS platforms, a solution containing six different lipid standards (HexCer, PC, PE, PEp, SM, and ST) was analyzed by both methods. For MALDI, matrices DHB and 9-AA were selected for the analysis of lipid standards in positive and negative ion mode, respectively. A range of laser fluences were tested to determine the optimal signal intensity of intact lipid standards, with careful consideration to minimize laser-induced fragmentation. It was found that 16 mJ/cm² provided the optimal laser fluence for MALDI-MS analysis. Mass spectra for MALDI-MS analysis were acquired using the crystal positioning system function of the instrument, with a total of 20 scans collected and averaged (Figure 1c,d). Similarly, for NAPA, a range of laser fluences were tested to identify the optimal level for detection of intact ions from the lipid standards. It was determined that laser fluence 48 mJ/cm² provided the optimal signal intensity and minimum
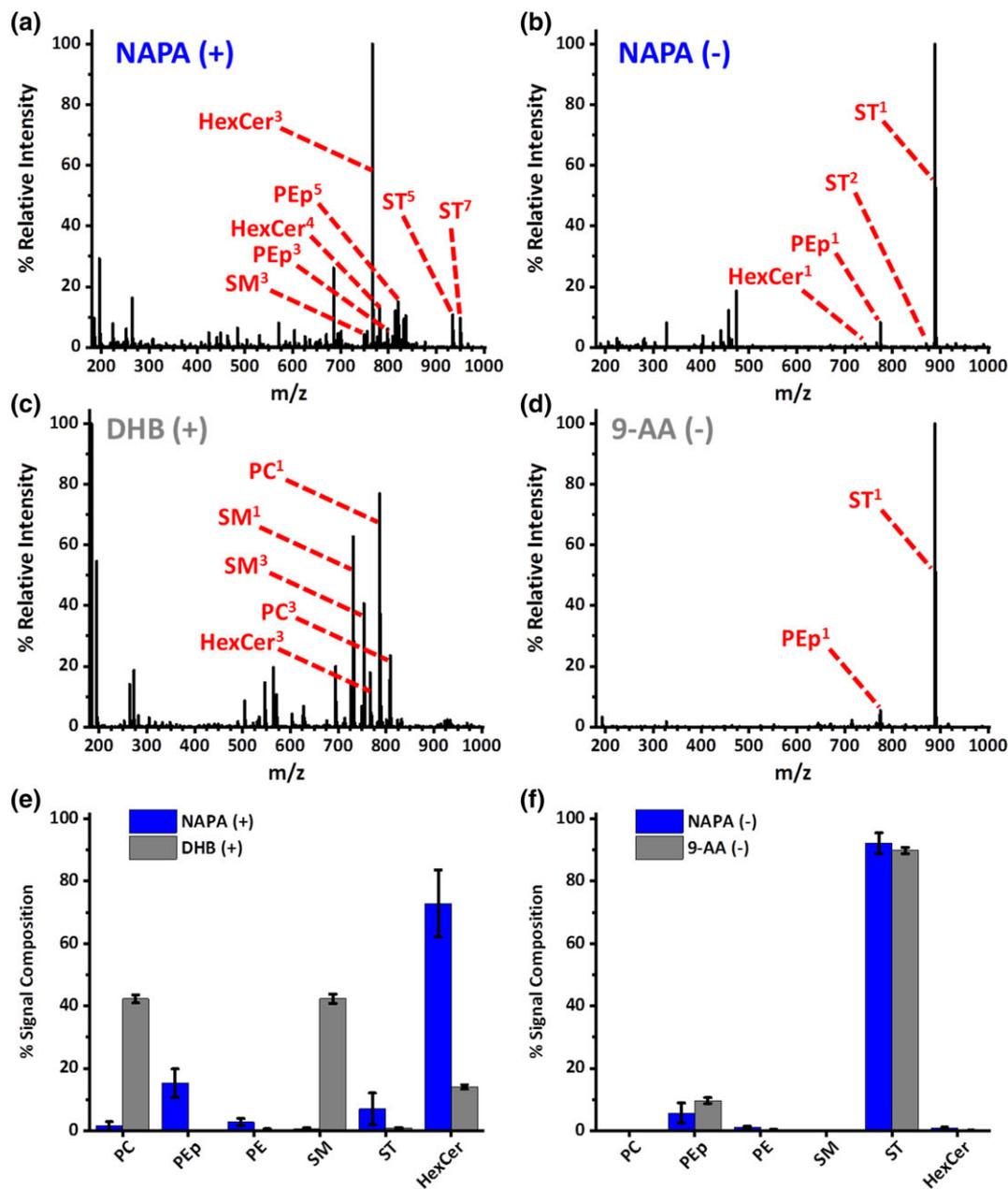
FIGURE 1 NAPA- and MALDI-MS analysis of lipid standard mixtures. Positive ion mode spectra from (a) NAPA and (c) MALDI (matrix: DHB) and negative ion mode spectra (b) NAPA and (d) MALDI (matrix: 9-AA) with detected lipids annotated. Bar graphs (e) and (f) compare MS intensities of lipid standards as a percentage of total assigned lipid signal. Superscripts for positive ion annotation indicate the ionic form: 1: [M+H]⁺, 2: [M-H₂O+H]⁺, 3: [M+Na]⁺, 4: [M+K]⁺, 5: [M+2Na-H]⁺, 6: [M+2K-H]⁺, and 7: [M+Na+K-H]⁺. Superscripts for negative ion mode annotation correspond to: 1: [M-H]⁻, and 2: [M-H₂O-H]⁻ [Color figure can be viewed at wileyonlinelibrary.com]
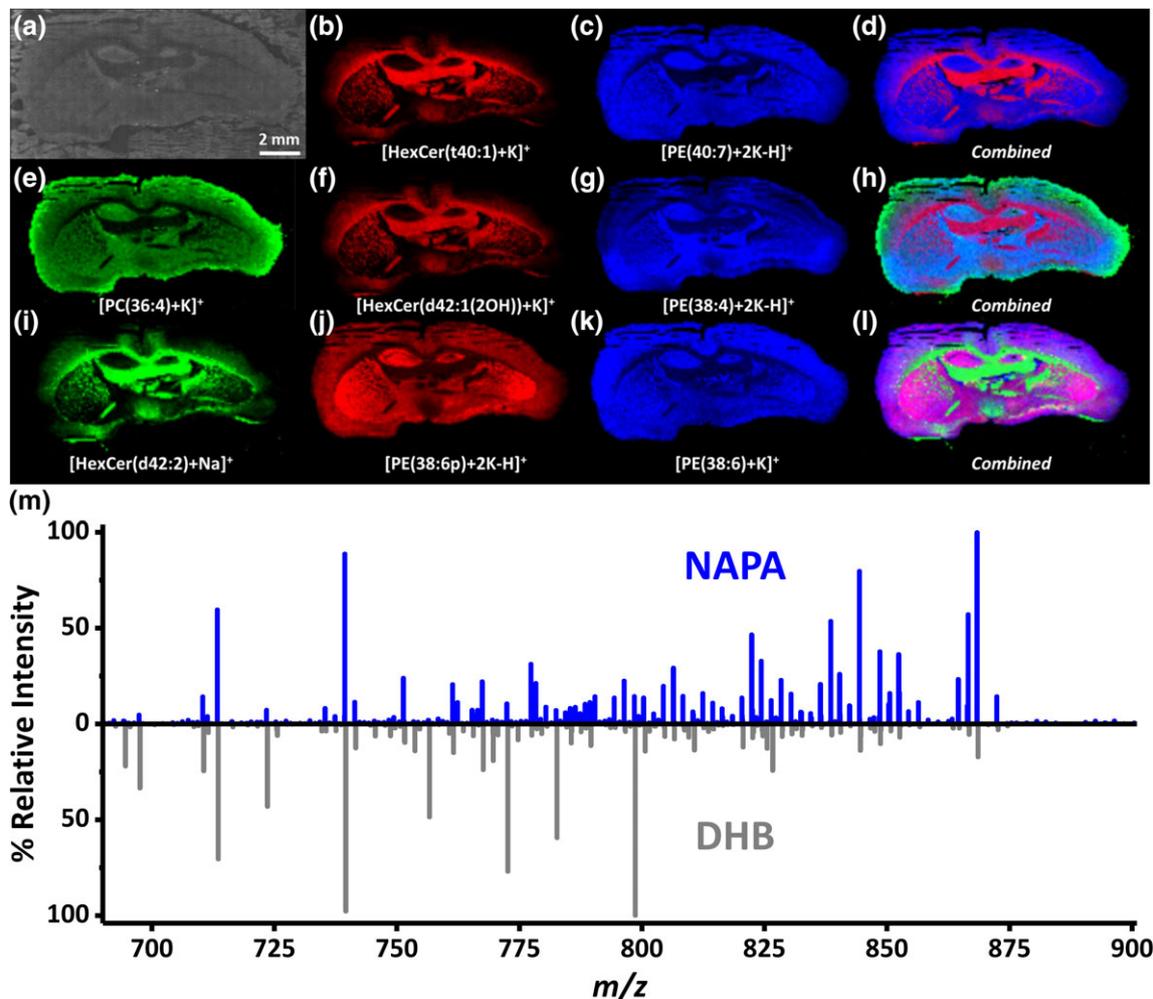
FIGURE 2 (a) Optical image of 10-µm thick coronal mouse brain section on NAPA. Positive ion mode chemical images (b), (c), (e), (f), (g), (i), (j), and (k) show distributions of selected ion signals, whereas (d), (h), and (l) indicate distributions combined from molecular images to their left. (m) Comparison of *m/z* region 690 to 900 from NAPA-LDI-MSI and MALDI-MSI averaged over entire adjacent mouse brain tissue sections [Color figure can be viewed at wileyonlinelibrary.com]

fragmentation. Using the tissue imaging function of the instrument, the location of the deposited lipid standards on the NAPA chip was registered, and mass spectra were acquired. A total of 20 orbitrap scans were averaged from areas where reliable lipid signal was found (Figure 1a,b).

Comparison of the detected lipid standards (Figure 1) in positive and negative ion modes provided key insights into the selectivity of NAPA- and MALDI-MS platforms for the ionization of different lipid classes. In Figure 1a, NAPA was found to favor ionization of HexCer, PE, and ST in positive ion mode, with these species accounting for 73, 18, and 7%, respectively, of the total assigned lipid signal. In Figure 1c, MALDI, by contrast, favored ionization of PC and SM, with both lipids accounting for 42% of the total assigned lipid signal. In negative ion mode, ST was the dominant lipid species detected by both NAPA (Figure 1b) and MALDI (Figure 1d) platforms, representing 92 and 90% of the assigned lipid signal, respectively.

To compare the coverage of lipids provided by the NAPA-LDI-MSI and MALDI-MSI platforms on real-world samples, mouse brain tissue sections were imaged at 100 µm spatial resolution in both positive and negative ion modes. For MALDI tissue imaging experiments,

matrices DHB and 9-AA were selected for positive and negative ion modes, respectively. As performed with the analysis of lipid standards, the laser fluence and number of laser shots/scan were determined by systematically varying each parameter until optimal signal of the detected intact lipid species were observed. It was found that MALDI-MSI and NAPA-LDI-MSI tissue imaging experiments had the same optimal laser fluence of 120 mJ/cm^2, with 10 laser shots/scan and 3 laser shots/scan, respectively. For comparative analysis in positive ion mode, 10 µm-thick serial coronal mouse brain sections were taken starting approximately −2 mm from the bregma. For negative ion mode, serial tissue sections were taken approximately −6 mm from the bregma.

Comparison of mass spectra for the *m/z* 690 to 900 region for NAPA-LDI-MSI and MALDI-MSI averaged over the entire mouse brain tissue sections can be found in Figure 2m. For MALDI, the higher intensity peaks found in the *m/z* 700–800 region correspond to lipid classes PC and PA. In NAPA, the higher intensity peaks are found in the *m/z* 800–875 region, corresponding to lipid classes HexCer and PE.
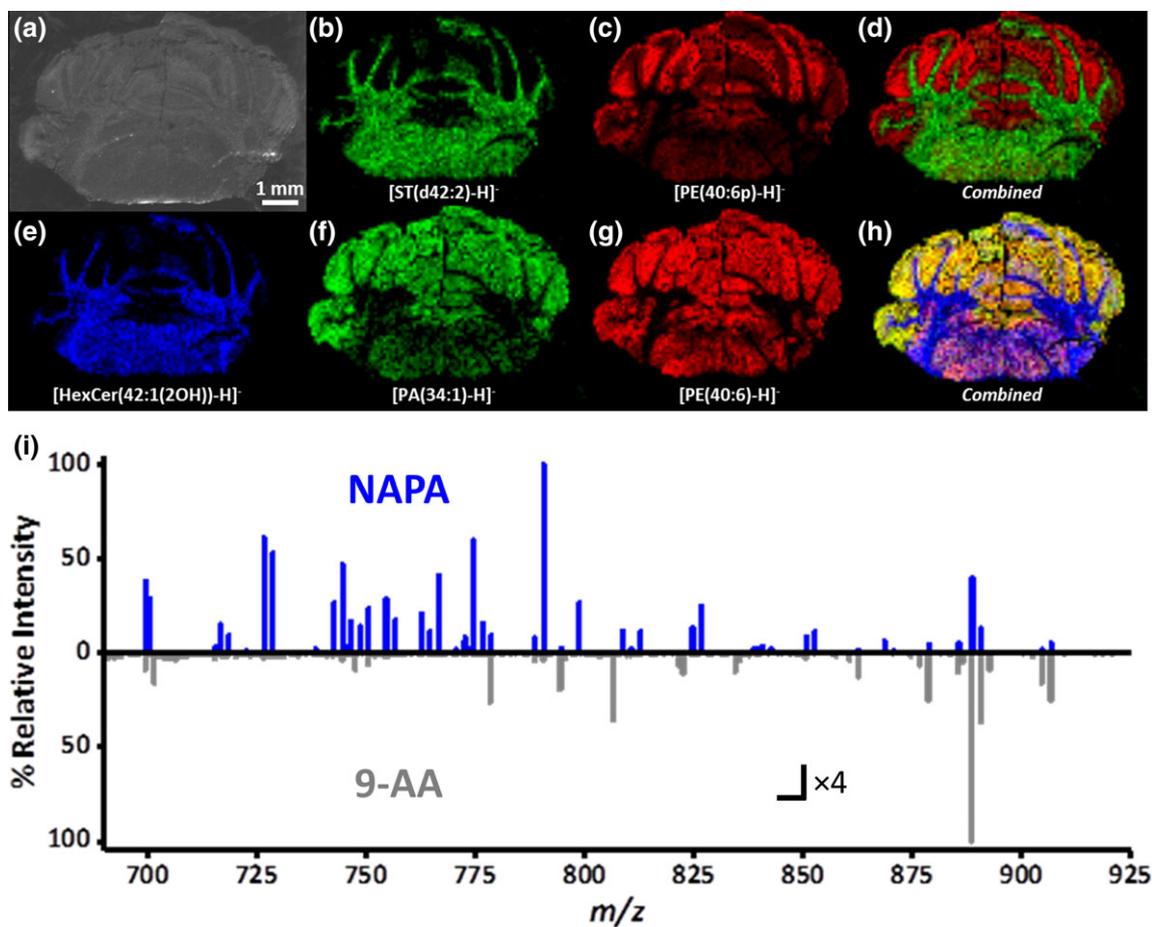
FIGURE 3 (a) Optical image of 10-μm thick coronal mouse brain section on NAPA. Negative ion mode chemical images (b), (c), (e), (f), and (g) show distributions of selected ion signals, whereas (d) and (h) indicate distributions combined from molecular images to their left. (m) Comparison of *m/z* region 690 to 900 from NAPA-LDI-MSI and MALDI-MSI averaged over entire adjacent mouse brain tissue sections [Color figure can be viewed at wileyonlinelibrary.com]

As observed in the chemical images found in Figures 2b–l, NAPA-LDI-MSI identified the localization of the HexCer and PE lipid classes. For example, it was found that HexCer lipids were more strongly detected in the corpus callosum, and certain parts of hippocampal formation and the thalamus. Lipids such as PE and PEp were more evenly distributed to areas such as the cerebral cortex, including the hippocampal formation, cerebral nuclei, hypothalamus, and certain parts of the thalamus. The combined images found in Figure 2d, h, and l, which are composed of the red, green, and blue values of each pixel in the molecular images to their left, allow for the identification of the dominant lipids in particular anatomical regions of the tissue sections.

A comparison of the acquired negative ion mass spectra in the *m/z* 690 to 900 region, averaged for the entire tissue section (Figure 3i), revealed that MALDI favored the ionization of ST lipids, found in the *m/z* 850–900 region, whereas NAPA favored the ionization of lipid classes HexCer and PE in the *m/z* 775–850 region.

Chemical images from NAPA-LDI-MSI in negative ion mode (Figures 3b-h) revealed HexCer, PE, and ST to be the dominant detected lipid classes, with HexCer and ST being localized to the arbor vitae in the cerebellum, as well as the medulla. In contrast, PE (40:6) was found to be localized to both the cerebellar cortex, and to a lesser extent, the medulla (Figure 3g). A corresponding plasmalogen, PE

(40:6p), was predominantly found in the cerebellar cortex (Figure 3c). The combined images in Figure 3d, h, which are combined from the chemical images to their left, highlight the specific regions where individual lipids dominate among the species detected in these experiments.

For a more in-depth comparison of lipid signal intensities and molecular coverage, spectra from the same region of the brain tissue were taken and analyzed by both the NAPA and MALDI platforms. In positive ion mode, five adjacent MS scans (1 pixel/scan) localized to the cortex were compared. In negative ion mode, due to the overall lower signal, four averaged MS scans (1 scan/pixel) from five adjacent areas localized to the medulla were compared. In positive ion mode (Figure 4a), the signal intensity is considerably stronger for NAPA compared to MALDI, especially for HexCer, PE, and PA. In negative ion mode, ion intensities are higher for MALDI, in particular for PC, FA, and ST, but NAPA signal was still superior for PE lipids (Figure 4b).

The molecular coverage provided by these two MSI platforms is compared in Figure 4c,d. As observed in the analysis of lipid standards, NAPA-LDI-MSI provided increased coverage of lipid classes PE and HexCer, in both positive and negative ion modes, relative to MALDI-MSI (Figure 4c,d). For example, in positive ion mode, HexCer, PE, PC,
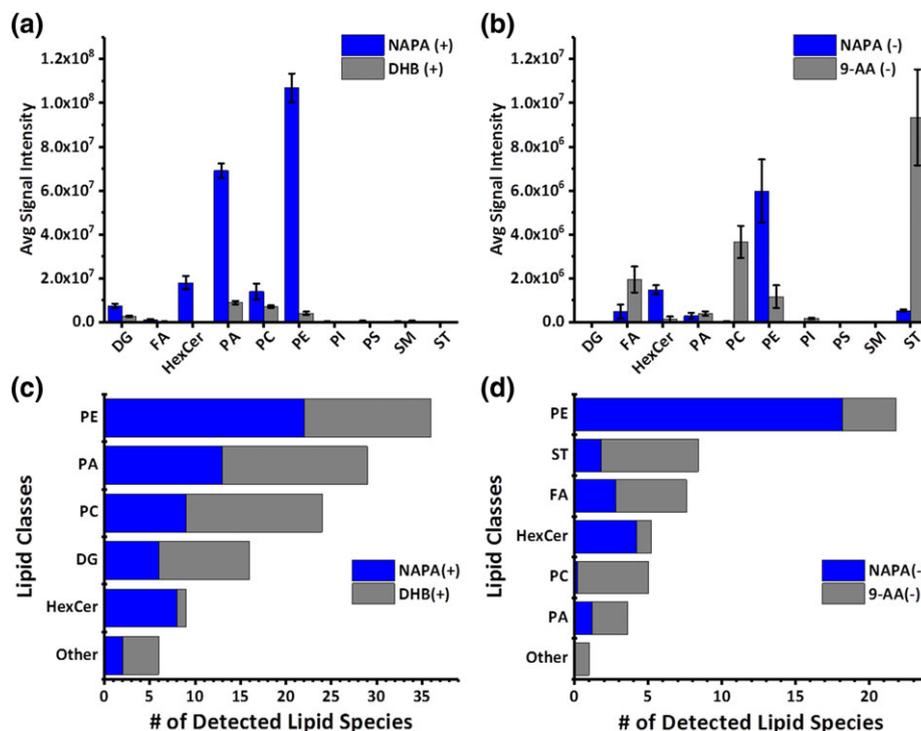
FIGURE 4 Comparison of lipid detection for NAPA- and MALDI-MSI of coronal mouse brain tissue sections in positive and negative ion mode. (a) Relative intensities of lipid species detected from cortex of mouse brain tissue sections in positive ion mode. (b) Relative intensities of lipids detected from medulla of mouse brain tissue sections in negative ion mode. (c) and (d) Number of lipid species detected per class in positive and negative ion modes, respectively [Color figure can be viewed at wileyonlinelibrary.com]

and PA were represented in the NAPA spectra by 8, 22, 9, and 13, species, respectively, whereas in the MALDI spectra the same lipids were present at 1, 14, 15, and 16, respectively. In negative ion mode, the number of HexCer, PE, PC, PA, FA, and ST species detected by NAPA were 4, 18, 0, 1, 3, and 2, respectively, whereas MALDI identified 1, 4, 5, 2, 5, and 7 species, respectively. The complete list of confirmed and tentatively assigned lipids detected between both platforms can be found in Tables 1 and 2.

4 | DISCUSSION

Currently, an extensive amount of MALDI-MSI studies exists that have investigated lipids in mouse brain tissue sections, demonstrating remarkable capabilities for the detection and imaging of phospholipids such as PC, PI, PE, and PS (Burnum et al., 2009; Murphy, Hankin, & Barkley, 2009; Puolitaival, Burnum, Cornett, & Caprioli, 2008). Furthermore, MALDI-MSI has been used to detect and spatially map out changes in natural abundances of PC and ST lipid classes in a mouse model of Alzheimer's disease (Hong et al., 2016). To help enhance the ionization efficiency of MALDI-MSI with respect to sphingolipid species such as HexCer and Cer, silver nanoparticles and sub-micron dopamine-modified TiO_2 particles have been used to image and monitor changes of sphingolipid levels in traumatic brain injuries and age-dependent studies, respectively (Roux et al., 2016; Wu, Chu, Rubakhin, Gillette, & Sweedler, 2017). Gangliosides, another class of lipids known to be extremely important in the CNS, have also been imaged using MALDI (Colsch & Woods, 2010; Skraskova et al., 2016).

The ability to reveal distributions of complementary lipid classes such as PE, PEp, and HexCer in brain tissue by NAPA-LDI-MSI offers a number of interesting possibilities for further investigations and applications. For example, tumor suppressor gene, p53, when mutated has been linked to multiple brain cancers such as astrocytoma and glioblastoma (Watanabe et al., 1997; Watanabe, Sato, Yonekawa, Kleihues, & Ohgaki, 1996). Lipidomics studies investigating the p53 genetic mutation found statistically significant changes in PEp and HexCer levels localized to areas of cancerous brain tissue such as the hypothalamus and hippocampus (Lee et al., 2016). Additionally, terminal neurological diseases such as Alzheimer's disease have been found to result in significant decreases in PE and increases in HexCer localized to the prefrontal cortex (Chan et al., 2012). Reduced levels of PEp in the cortex have also been associated with Alzheimer's disease and adrenoleukodystrophy, a debilitating neurological disease (Grimm et al., 2011; Khan, Singh, & Singh, 2008). With its enhanced ionization of these lipid species, NAPA-LDI-MSI has the potential to provide additional insight into these highly localized metabolic disruptions and their role in disease progression.

The underlying reason for the enhanced ionization of certain lipid classes by NAPA-LDI-MS compared to the tested MALDI-MS matrices is not immediately clear. However, we hypothesize that the mechanisms of material removal and the composition of the desorption plume are significant factors. In MALDI-MSI, the tissue section is adhered to a surface and the matrix droplets are deposited on top of it. As the matrix solution dries, analytes from the tissue are extracted and they co-crystallize with the matrix material. When irradiated, the matrix volatilizes and a comparatively small amount of the analyte

TABLE 1 Metabolite and lipid assignments based on accurate mass (≤5 ppm mass error) for positive ion mode MSI analysis of mouse brain sections. Acyl chain compositions are reported for lipids identified in parallel by LC-MS/MS analysis

Compound identification	Fatty acids from LC-MSMS	Chemical formula	Ionic species	Calc. m/z	NAPA Δm (ppm)	MALDI Δm (ppm)
ADP		$C_{10}H_{15}N_5O_{10}P_2$	$[M-H_2O+H]^+$	410.0261	x	1.7
			$[M+H]^+$	428.0367	x	2
			$[M+Na]^+$	450.0186	x	1.8
			$[M+K]^+$	465.9926	x	2.2
			$[M+Na+K-H]^+$	487.9745	x	1.7
			$[M+2K-H]^+$	503.9485	x	2.3
Carnitine (18:1)		$C_{25}H_{47}NO_4$	$[M+2K-H]^+$	502.2696	0.4	x
Carnitine (18:2)		$C_{25}H_{45}NO_4$	$[M+2K-H]^+$	500.2539	−0.4	x
Cer (36:1)	d18:1, 18:0	$C_{36}H_{71}NO_3$	$[M-H_2O+H]^+$	548.5401	1.9	1.8
			$[M+Na]^+$	588.5326	1.5	1.1
			$[M+K]^+$	604.5066	2.3	2.2
Cer (d34:1)		$C_{34}H_{67}NO_3$	$[M+K]^+$	576.4753	2.9	x
Cer (d38:1)		$C_{38}H_{75}NO_3$	$[M+K]^+$	632.5379	2.2	x
Cer (d40:2)		$C_{40}H_{77}NO_3$	$[M-H_2O+H]^+$	602.5871	x	2.3
			$[M+H]^+$	620.5976	x	2.5
			$[M+K]^+$	658.5535	3	x
Cer (d42:1)		$C_{42}H_{83}NO_3$	$[M-H_2O+H]^+$	632.6340	x	3.8
Cer (d42:2)		$C_{42}H_{81}NO_3$	$[M-H_2O+H]^+$	630.6184	1.9	2.7
			$[M+H]^+$	648.6289	x	2.5
			$[M+Na]^+$	670.6109	−1.5	x
			$[M+K]^+$	686.5848	3.8	x
CerP (d18:1/18:1)		$C_{36}H_{70}N_1O_6P$	$[M+Na]^+$	666.4833	x	1.3
			$[M+K]^+$	682.4572	x	2.4
Cholesterol (—H_2O)		$C_{27}H_{44}$	$[M+H]^+$	369.3516	0.2	1.2
DG (34:1)		$C_{37}H_{70}O_5$	$[M-H_2O+H]^+$	577.5190	1.7	1.7
			$[M+K]^+$	633.4855	2.9	x
DG (34:2)		$C_{37}H_{68}O_5$	$[M-H_2O+H]^+$	575.5034	3.4	4.5
			$[M+K]^+$	631.4698	2.8	x
DG (36:1)		$C_{39}H_{74}O_5$	$[M-H_2O+H]^+$	605.5503	2.3	1.7
			$[M+Na]^+$	645.5429	−0.1	x
			$[M+K]^+$	661.5168	2.9	x
			$[M+2K-H]^+$	699.4727	2.2	x
DG (36:2)		$C_{39}H_{72}O_5$	$[M-H_2O+H]^+$	603.5347	2.5	2.4
			$[M+K]^+$	659.5011	2.6	x
DG (36:3)		$C_{39}H_{70}O_5$	$[M-H_2O+H]^+$	601.5190	2.7	3
			$[M+K]^+$	657.4855	3	x
DG (36:4)		$C_{39}H_{68}O_5$	$[M-H_2O+H]^+$	599.5034	−1.3	−1.8
			$[M+K]^+$	655.4698	2.8	x
DG (38:1)		$C_{41}H_{78}O_5$	$[M-H_2O+H]^+$	633.5816	2.3	2.8
			$[M+K]^+$	689.5481	3	x
DG (38:3)		$C_{41}H_{74}O_5$	$[M+2Na-H]^+$	691.5248	−0.6	x
DG (38:4)	18:0, 20:4	$C_{41}H_{72}O_5$	$[M-H_2O+H]^+$	627.5347	1.7	−0.1
			$[M+Na]^+$	667.5272	−1.4	x
			$[M+K]^+$	683.5011	2.9	x
DG (38:5)		$C_{41}H_{70}O_5$	$[M-H_2O+H]^+$	625.5190	1.7	−0.2
			$[M+K]^+$	681.4855	1.5	0.4
DG (38:6)		$C_{41}H_{68}O_5$	$[M-H_2O+H]^+$	623.5034	2.7	3.3
			$[M+K]^+$	679.4698	2.6	x
DG (40:4)		$C_{43}H_{76}O_5$	$[M-H_2O+H]^+$	655.5660	2.5	2.2
DG (40:5)		$C_{43}H_{74}O_5$	$[M+2K-H]^+$	747.4727	2.1	x

TABLE 1 (Continued)

Compound identification	Fatty acids from LC-MSMS	Chemical formula	Ionic species	Calc. *m/z*	NAPA Δm (ppm)	MALDI Δm (ppm)
DG (40:9)		$C_{43}H_{66}O_5$	$[M-H_2O+H]^+$	645.4877	−1.9	−2.1
			$[M+K]^+$	701.4542	0.4	x
			$[M+Na+K-H]^+$	723.4361	1	0.7
			$[M+2K-H]^+$	739.4101	1.2	2.3
DG (42:9)		$C_{45}H_{70}O_5$	$[M-H_2O+H]^+$	673.5190	−1.8	−1.5
			$[M+H]^+$	691.5296	x	−0.1
FA (12:0)		$C_{12}H_{24}O_2$	$[M+2K-H]^+$	277.0967	x	0.8
FA (14:0)		$C_{14}H_{28}O_2$	$[M+Na]^+$	251.1982	x	0.4
			$[M+2K-H]^+$	305.1280	x	−1.9
FA (14:1)		$C_{14}H_{26}O_2$	$[M+2K-H]^+$	303.1123	x	−0.6
FA (15:0)		$C_{15}H_{30}O_2$	$[M+Na]^+$	265.2138	x	0.3
FA (16:0)		$C_{16}H_{32}O_2$	$[M-H_2O+H]^+$	239.2369	x	−2.9
			$[M+H]^+$	257.2475	x	0.7
			$[M+Na]^+$	279.2295	−0.7	0.5
			$[M+K]^+$	295.2034	x	−0.1
			$[M+2Na-H]^+$	301.2114	−0.2	1.9
			$[M+Na+K-H]^+$	317.1853	−0.4	2.4
			$[M+2K-H]^+$	333.1593	−0.3	1.9
FA (16:1)		$C_{16}H_{30}O_2$	$[M-H_2O+H]^+$	237.2213	x	−2
			$[M+Na]^+$	277.2138	x	1.2
			$[M+2Na-H]^+$	299.1958	x	3.7
FA (18:0)		$C_{18}H_{36}O_2$	$[M-H_2O+H]^+$	267.2682	x	1
			$[M+Na]^+$	307.2608	−0.3	0.7
			$[M+K]^+$	323.2347	−0.4	x
			$[M+2Na-H]^+$	329.2427	−0.4	1.6
			$[M+Na+K-H]^+$	345.2166	0.5	x
			$[M+2K-H]^+$	361.1906	0.2	0.8
FA (18:1)		$C_{18}H_{34}O_2$	$[M-H_2O+H]^+$	265.2526	−1.3	0.7
			$[M+H]^+$	283.2632	x	0.3
			$[M+Na]^+$	305.2451	−1.1	0.8
			$[M+K]^+$	321.2190	−0.5	x
			$[M+2K-H]^+$	359.1749	0	4.1
FA (18:2)		$C_{18}H_{32}O_2$	$[M-H_2O+H]^+$	263.2369	x	1.1
			$[M+Na]^+$	303.2295	x	0.9
FA (18:3)		$C_{18}H_{30}O_2$	$[M+2K-H]^+$	355.1436	x	4.8
FA (20:4)		$C_{20}H_{32}O_2$	$[M+Na]^+$	327.2295	−0.7	−1.1
			$[M+K]^+$	343.2034	−0.5	x
			$[M+2Na-H]^+$	349.2114	1	5
			$[M+Na+K-H]^+$	365.1853	1.4	x
			$[M+2K-H]^+$	381.1593	0.3	2.9
FA (22:6)		$C_{22}H_{32}O_2$	$[M+Na]^+$	351.2295	0.2	0.4
			$[M+K]^+$	367.2034	−0.3	−0.2
			$[M+2Na-H]^+$	373.2114	0.4	1.5
			$[M+Na+K-H]^+$	389.1853	0.8	−3.4
			$[M+2K-H]^+$	405.1593	0.3	1.5
HexCer (d42:1)		$C_{48}H_{93}NO_8$	$[M+Na]^+$	834.6793	1.7	1.5
			$[M+K]^+$	850.6533	−1.8	x
HexCer (d42:2)		$C_{48}H_{91}NO_8$	$[M-H_2O+H]^+$	792.6712	x	3.4
			$[M+Na]^+$	832.6637	3.5	2
			$[M+K]^+$	848.6376	1	x
			$[M+2K-H]^+$	886.5935	−4.6	x

TABLE 1 (Continued)

Compound identification	Fatty acids from LC-MSMS	Chemical formula	Ionic species	Calc. m/z	NAPA Δm (ppm)	MALDI Δm (ppm)
HexCer (d40:0)		$C_{46}H_{91}NO_8$	$[M+K]^+$	824.6376	x	−1.3
			$[M+Na+K-H]^+$	846.6196	4.1	x
HexCer (d36:1)		$C_{42}H_{81}NO_8$	$[M+Na]^+$	750.5854	2.4	2.8
			$[M+K]^+$	766.5594	2.8	4.3
HexCer (d38:1)		$C_{44}H_{85}NO_8$	$[M+Na]^+$	778.6167	−0.3	x
			$[M+K]^+$	794.5907	2.1	x
HexCer (d40:1)		$C_{46}H_{89}NO_8$	$[M+Na]^+$	806.6480	2.2	2.6
HexCer (d41:1)		$C_{47}H_{91}NO_8$	$[M+2K-H]^+$	874.5935	1.4	x
			$[M+K]^+$	848.6376	x	1.2
HexCer (d34:2)		$C_{40}H_{75}NO_8$	$[M+K]^+$	736.5124	3.5	x
HexCer (d40:2)		$C_{46}H_{87}NO_8$	$[M+Na]^+$	804.6324	2.9	x
			$[M+K]^+$	820.6063	1.2	x
HexCer (d41:2)		$C_{47}H_{89}NO_8$	$[M+2Na-H]^+$	776.4393	−2.8	x
			$[M+Na]^+$	818.6480	4.2	x
			$[M+K]^+$	834.6220	−0.8	x
HexCer (d40:1[2OH])		$C_{46}H_{89}NO_9$	$[M+K]^+$	838.6169	x	2
HexCer (d36:1[2OH])		$C_{42}H_{81}NO_9$	$[M+K]^+$	782.5543	2.8	x
HexCer (d38:1[2OH])		$C_{44}H_{85}NO_9$	$[M+Na]^+$	794.6117	x	−0.7
			$[M+K]^+$	810.5856	2.1	x
HexCer (d42:1[2OH])		$C_{48}H_{93}NO_9$	$[M+Na]^+$	850.6743	x	3.9
			$[M+K]^+$	866.6482	1.3	3
			$[M+2K-H]^+$	904.6041	2.9	x
HexCer (d38:2[2OH])		$C_{44}H_{83}NO_9$	$[M+K]^+$	808.5700	1	x
HexCer (d37:2[2OH])		$C_{43}H_{81}NO_9$	$[M+K]^+$	794.5543	−2.8	x
HexCer (d40:2[2OH])		$C_{46}H_{87}NO_9$	$[M+Na]^+$	820.6273	x	−3.1
HexCer (d42:2[2OH])		$C_{48}H_{91}NO_9$	$[M+K]^+$	864.6326	1.4	2.3
			$[M+2K-H]^+$	902.5884	4.4	x
HexCer (d43:2[2OH])		$C_{49}H_{93}NO_9$	$[M+K]^+$	878.6482	5	x
HexCer (t34:1[2OH])		$C_{40}H_{77}NO_{10}$	$[M+Na+K-H]^+$	792.4999	3.8	x
HexCer (t36:1[2OH])		$C_{42}H_{81}NO_{10}$	$[M+Na+K-H]^+$	820.5312	−3.5	x
			$[M+2K-H]^+$	836.5051	x	1.2
HexCer (t38:1[2OH])		$C_{44}H_{85}NO_{10}$	$[M+Na+K-H]^+$	848.5625	−2.2	x
Glutamate		$C_5H_9NO_4$	$[M+K]^+$	186.0163	−2.7	x
			$[M+2Na-H]^+$	192.0243	x	0
			$[M+Na+K-H]^+$	207.9983	x	0.2
			$[M+2K-H]^+$	223.9722	−3	0.9
Glutamine		$C_5H_{10}N_2O_3$	$[M+K]^+$	185.0323	−2.8	0.2
			$[M+2Na-H]^+$	191.0403	x	−0.9
			$[M+Na+K-H]^+$	207.0143	−1	0.8
			$[M+2K-H]^+$	222.9882	−0.5	0.9
Heme		$FeC_{34}H_{33}N_4O_5$	$[M-H_2O+H]^+$	616.1767	x	3.7
HexCer (t40:1)		$C_{46}H_{89}NO_9$	$[M+Na]^+$	822.6430	3.5	3.4
			$[M+K]^+$	838.6169	2.7	x
Hexose-bisphosphate		$C_6H_{14}O_{12}P_2$	$[M-H_2O+H]^+$	322.9928	x	2
Hexose-phosphate		$C_6H_{13}O_9P$	$[M-H_2O+H]^+$	243.0264	x	−2.3
			$[M+H]^+$	261.0370	x	−2.1
			$[M+Na]^+$	283.0189	x	2.7
			$[M+K]^+$	298.9929	x	2.1
LysoPC (14:0)		$C_{22}H_{46}NO_7P$	$[M+Na+K-H]^+$	528.2463	−4	1.4
			$[M+2K-H]^+$	544.2202	0.7	1.8

TABLE 1 (Continued)

Compound identification	Fatty acids from LC-MSMS	Chemical formula	Ionic species	Calc. m/z	NAPA Δm (ppm)	MALDI Δm (ppm)
LysoPC (16:0)		$C_{24}H_{50}NO_7P$	$[M-H_2O+H]^+$	478.3292	1.1	1.2
			$[M+H]^+$	496.3398	x	1.6
			$[M+Na]^+$	518.3217	x	0.9
			$[M+K]^+$	534.2957	x	1
			$[M+2K-H]^+$	572.2515	0.4	x
LysoPC (18:0)		$C_{26}H_{54}NO_7P$	$[M-H_2O+H]^+$	506.3605	x	2.4
			$[M+H]^+$	524.3711	x	2.3
			$[M+Na]^+$	546.3530	x	2.2
			$[M+K]^+$	562.3270	x	0.7
LysoPC (18:2)		$C_{26}H_{50}NO_7P$	$[M-H_2O+H]^+$	502.3292	x	−3.7
			$[M+K]^+$	558.2957	x	3.9
			$[M+Na+K-H]^+$	580.2776	2.3	x
LysoPC (22:0)		$C_{30}H_{62}NO_7P$	$[M+H]^+$	580.4337	x	−4.3
LysoPC (22:4)		$C_{30}H_{54}NO_7P$	$[M+2Na-H]^+$	616.3350	4.8	x
			$[M+Na+K-H]^+$	632.3089	4.1	x
			$[M+2K-H]^+$	648.2828	4.6	x
LysoPC (22:5)		$C_{30}H_{52}NO_7P$	$[M+K]^+$	608.3113	−0.9	x
			$[M+2Na-H]^+$	614.3193	x	−1
LysoPE (16:0)		$C_{21}H_{44}NO_7P$	$[M+2K-H]^+$	530.2046	x	0.3
LysoPE (16:1)		$C_{21}H_{42}NO_7P$	$[M+2K-H]^+$	528.1889	x	3.2
LysoPE (18:0)		$C_{23}H_{48}NO_7P$	$[M+2Na-H]^+$	526.2880	x	1.1
			$[M+Na+K-H]^+$	542.2620	x	0.3
			$[M+2K-H]^+$	558.2359	0.9	1
LysoPE (18:1)		$C_{23}H_{46}NO_7P$	$[M+K]^+$	518.2644	x	3.6
			$[M+2K-H]^+$	556.2202	0.6	1.8
LysoPE (20:0)		$C_{25}H_{52}NO_7P$	$[M-H_2O+H]^+$	492.3449	x	0.6
			$[M+H]^+$	510.3554	x	0.5
LysoPE (20:1)		$C_{25}H_{50}NO_7P$	$[M+K]^+$	546.2957	x	3.9
			$[M+2K-H]^+$	584.2515	3.5	x
LysoPE (20:2)		$C_{25}H_{48}NO_7P$	$[M+2K-H]^+$	582.2359	3	x
LysoPE (20:4)		$C_{25}H_{44}NO_7P$	$[M+2Na-H]^+$	546.2567	x	4.5
			$[M+Na+K-H]^+$	562.2307	4	2.1
			$[M+2K-H]^+$	578.2046	1.2	2.7
LysoPE (22:4)		$C_{27}H_{48}NO_7P$	$[M+K]^+$	568.2800	x	−0.5
			$[M+Na+K-H]^+$	590.2620	x	4.1
			$[M+2K-H]^+$	606.2359	x	4.2
LysoPE (22:6)		$C_{27}H_{44}NO_7P$	$[M+K]^+$	564.2487	4.5	2.8
			$[M+2Na-H]^+$	570.2567	x	1.1
			$[M+Na+K-H]^+$	586.2307	x	2.4
			$[M+2K-H]^+$	602.2046	2.7	3
LysoPE (24:6)		$C_{29}H_{48}NO_7P$	$[M+Na]^+$	576.3061	x	−4.6
			$[M+K]^+$	592.2800	1.3	x
LysoPG (16:0)		$C_{22}H_{45}O_9P$	$[M-H_2O+H]^+$	467.2768	0.2	x
LysoPI (18:0)		$C_{27}H_{53}O_{12}P$	$[M+2Na-H]^+$	645.2986	−3.3	x
LysoPI (18:1)		$C_{27}H_{51}O_{12}P$	$[M+Na]^+$	621.3010	−1.6	x
			$[M+K]^+$	637.2750	x	−1.6
			$[M+2Na-H]^+$	643.2830	1.2	x
PA (32:0)		$C_{35}H_{69}O_8P$	$[M+2K-H]^+$	725.3921	x	2.7
PA (32:1)		$C_{35}H_{67}O_8P$	$[M+K]^+$	685.4205	3.3	3.4
PA (34:1)		$C_{37}H_{71}O_8P$	$[M+Na]^+$	697.4779	1.7	x
			$[M+K]^+$	713.4518	3.1	2
			$[M+2K-H]^+$	751.4077	3.3	2.8

TABLE 1 (Continued)

Compound identification	Fatty acids from LC-MSMS	Chemical formula	Ionic species	Calc. m/z	NAPA Δm (ppm)	MALDI Δm (ppm)
PA (34:3)		$C_{37}H_{67}O_8P$	$[M+Na]^+$	693.4466	x	0.2
			$[M+K]^+$	709.4205	2.3	0.2
			$[M+2K-H]^+$	747.3764	x	1.4
PA (34:4)		$C_{37}H_{65}O_8P$	$[M+H]^+$	669.4490	x	2.2
PA (36:0)		$C_{39}H_{77}O_8P$	$[M-H_2O+H]^+$	687.5323	3.1	x
PA (36:1)		$C_{39}H_{75}O_8P$	$[M+2K-H]^+$	779.4390	x	3.2
PA (36:2)		$C_{39}H_{73}O_8P$	$[M-H_2O+H]^+$	683.5010	x	−0.8
			$[M+Na]^+$	723.4935	2.7	x
			$[M+K]^+$	739.4675	3	2.3
			$[M+2K-H]^+$	777.4234	2.8	2.6
PA (36:3)		$C_{39}H_{71}O_8P$	$[M+Na]^+$	721.4779	0.2	x
			$[M+K]^+$	737.4518	4.2	2.7
PA (36:4)		$C_{39}H_{69}O_8P$	$[M+H]^+$	697.4803	x	−1.6
			$[M+Na]^+$	719.4622	x	0.1
			$[M+K]^+$	735.4362	0.2	0
			$[M+Na+K-H]^+$	757.4181	x	1.4
			$[M+2K-H]^+$	773.3921	x	2.1
PA (36:5)		$C_{39}H_{67}O_8P$	$[M+H]^+$	695.4646	x	−0.9
			$[M+K]^+$	733.4205	1.6	x
PA (36:6)		$C_{39}H_{65}O_8P$	$[M+K]^+$	731.4049	2.9	x
PA (38:2)		$C_{41}H_{77}O_8P$	$[M+K]^+$	767.4988	3.2	2.1
PA (38:3)		$C_{41}H_{75}O_8P$	$[M-H_2O+H]^+$	709.5167	x	−0.2
			$[M+K]^+$	765.4831	3	2.7
			$[M+2K-H]^+$	803.4390	3.4	x
PA (38:4)		$C_{41}H_{73}O_8P$	$[M-H_2O+H]^+$	707.5010	2.8	2.8
			$[M+H]^+$	725.5116	x	−0.2
			$[M+Na]^+$	747.4935	x	1.3
			$[M+K]^+$	763.4675	x	2.3
			$[M+2K-H]^+$	801.4234	x	1.4
PA (38:5)		$C_{41}H_{71}O_8P$	$[M-H_2O+H]^+$	705.4854	2.6	x
			$[M+H]^+$	723.4959	x	−1.4
			$[M+Na]^+$	745.4779	−1.5	1.4
			$[M+K]^+$	761.4518	1.5	1.3
			$[M+2K-H]^+$	799.4077	3.4	3.2
PA (38:6)		$C_{41}H_{69}O_8P$	$[M+H]^+$	721.4803	x	−1.3
			$[M+K]^+$	759.4362	2.8	0.8
			$[M+2K-H]^+$	797.3921	x	3
PA (38:7)		$C_{41}H_{67}O_8P$	$[M+K]^+$	757.4205	1.8	x
			$[M+2K-H]^+$	795.3764	2.8	2.1
PA (40:2)		$C_{43}H_{81}O_8P$	$[M+K]^+$	795.5301	x	−0.8
PA (40:5)		$C_{43}H_{75}O_8P$	$[M+H]^+$	751.5272	0	−0.7
			$[M+K]^+$	789.4831	0.7	1.3
			$[M+Na+K-H]^+$	811.4651	0.1	x
			$[M+2K-H]^+$	827.4390	−1.6	x
PA (40:6)		$C_{43}H_{73}O_8P$	$[M-H_2O+H]^+$	731.5010	0.6	−0.8
			$[M+H]^+$	749.5116	−1	−0.8
			$[M+K]^+$	787.4675	1.8	2.7
			$[M+Na+K-H]^+$	809.4494	x	1.1
			$[M+2K-H]^+$	825.4234	x	0.5
PA (40:7)		$C_{43}H_{71}O_8P$	$[M+K]^+$	785.4518	0.5	1.1
			$[M+Na+K-H]^+$	807.4338	x	3
			$[M+2K-H]^+$	823.4077	1.8	1.8

TABLE 1 (Continued)

Compound identification	Fatty acids from LC-MSMS	Chemical formula	Ionic species	Calc. m/z	NAPA Δm (ppm)	MALDI Δm (ppm)
PA (40:8)		$C_{43}H_{69}O_8P$	$[M-H_2O+H]^+$	727.4697	0.4	0
			$[M+K]^+$	783.4362	0.8	−0.5
			$[M+2K-H]^+$	821.3921	3.7	x
PA (42:7)		$C_{45}H_{75}O_8P$	$[M+K]^+$	813.4831	x	−0.4
PA (42:8)		$C_{45}H_{73}O_8P$	$[M-H_2O+H]^+$	755.5010	2.6	0.5
PA (44:12)		$C_{47}H_{69}O_8P$	$[M-H_2O+H]^+$	775.4697	2.1	x
			$[M+H]^+$	793.4803	x	1
			$[M+Na]^+$	815.4622	x	1.1
			$[M+K]^+$	831.4362	2.8	−4.5
PC (26:0)		$C_{34}H_{68}NO_8P$	$[M+Na+K-H]^+$	710.4134	x	−1.8
PC (32:1)	16:0, 16:1	$C_{40}H_{78}NO_8P$	$[M+K]^+$	770.5097	0.6	x
			$[M+Na+K-H]^+$	792.4916	x	0.5
			$[M+2K-H]^+$	808.4656	2	x
PC (32:3)		$C_{40}H_{74}NO_8P$	$[M+H]^+$	728.5225	x	−0.9
PC (34:1)		$C_{42}H_{82}NO_8P$	$[M+H]^+$	760.5851	x	2.4
			$[M+2K-H]^+$	836.4969	0.9	x
PC (34:2)	16:0, 18:2, 16:1, 18:1	$C_{42}H_{80}NO_8P$	$[M+K]^+$	796.5253	1	0.8
PC (34:3)		$C_{42}H_{78}NO_8P$	$[M+H]^+$	756.5538	−0.9	−1.1
PC (34:4)		$C_{42}H_{76}NO_8P$	$[M+H]^+$	754.5381	x	−1.5
PC (36:1)	16:0, 20:1, 18:0, 18:1	$C_{44}H_{86}NO_8P$	$[M+H]^+$	788.6164	x	2.7
			$[M+K]^+$	826.5723	3.1	2.1
			$[M+2K-H]^+$	864.5282	3.1	x
PC (36:2)	16:0, 20:2, 18:0, 18:2, 18:1, 18:1	$C_{44}H_{84}NO_8P$	$[M+K]^+$	824.5566	0.7	2
PC (36:4)	16:0, 20:4	$C_{44}H_{80}NO_8P$	$[M+H]^+$	782.5694	x	−0.8
			$[M+K]^+$	820.5253	3.6	1.3
			$[M+2K-H]^+$	858.4812	4.8	x
PC (36:5)	16:1, 20:4	$C_{44}H_{78}NO_8P$	$[M+H]^+$	780.5538	x	−1.4
PC (36:7)		$C_{44}H_{74}NO_8P$	$[M-H_2O+H]^+$	758.5119	0.9	1.4
PC (38:0)		$C_{46}H_{92}NO_8P$	$[M+2Na-H]^+$	862.6272	−2.7	−4.5
PC (38:1)	18:1, 20:0	$C_{46}H_{90}NO_8P$	$[M+K]^+$	854.6036	x	1.1
			$[M+Na+K-H]^+$	876.5855	−1.3	x
PC (38:2)	16:1, 22:1, 18:1, 20:1	$C_{46}H_{88}NO_8P$	$[M+Na]^+$	836.6140	−4.5	x
PC (38:4)	16:0, 22:4, 18:0, 20:4	$C_{46}H_{84}NO_8P$	$[M+H]^+$	810.6007	x	−0.7
			$[M+K]^+$	848.5566	x	2
PC (38:5)	16:0, 22:5, 18:1, 20:4	$C_{46}H_{82}NO_8P$	$[M+H]^+$	808.5851	x	−0.5
			$[M+Na]^+$	830.5670	x	0.6
			$[M+K]^+$	846.5410	x	2.7
PC (38:6)	16:0, 22:6	$C_{46}H_{80}NO_8P$	$[M+K]^+$	844.5253	x	2
PC (38:7)		$C_{46}H_{78}NO_8P$	$[M+H]^+$	804.5538	x	−1.2
PC (38:8)		$C_{46}H_{76}NO_8P$	$[M-H_2O+H]^+$	784.5276	1.7	0.9
PC (38:9)		$C_{46}H_{74}NO_8P$	$[M-H_2O+H]^+$	782.5119	4.3	x
PC (40:1)		$C_{48}H_{94}NO_8P$	$[M+K]^+$	882.6349	x	2.4
PC (40:4)	18:0, 22:4	$C_{48}H_{88}NO_8P$	$[M+K]^+$	876.5879	x	1.8
PC (40:6)	18:0, 22:6	$C_{48}H_{84}NO_8P$	$[M+Na]^+$	856.5827	x	1.6
			$[M+K]^+$	872.5566	4.5	2.1
PC (40:7)	18:1, 22:6, 20:3, 20:4	$C_{48}H_{82}NO_8P$	$[M+H]^+$	832.5851	x	−1.2
			$[M+K]^+$	870.5410	x	1.2
PC (40:8)		$C_{48}H_{80}NO_8P$	$[M+2K-H]^+$	906.4812	3.9	x
PC (42:1)	18:1, 24:0	$C_{50}H_{98}NO_8P$	$[M+K]^+$	910.6662	x	2.1
PC (42:3)		$C_{50}H_{94}NO_8P$	$[M+2Na-H]^+$	912.6429	x	−2
			$[M+Na+K-H]^+$	928.6168	−3.3	−3.3

TABLE 1 (Continued)

Compound identification	Fatty acids from LC-MSMS	Chemical formula	Ionic species	Calc. m/z	NAPA Δm (ppm)	MALDI Δm (ppm)
PC (42:4)		$C_{50}H_{92}NO_8P$	$[M+2Na-H]^+$	910.6272	−4.7	x
PC (42:5)		$C_{50}H_{90}NO_8P$	$[M+2Na-H]^+$	908.6116	−4.3	x
PC (44:10)		$C_{52}H_{84}NO_8P$	$[M+2K-H]^+$	958.5125	x	2.8
PC (46:6)		$C_{54}H_{96}NO_8P$	$[M+Na]^+$	940.6766	x	−4.5
PE (36:0p)		$C_{41}H_{82}NO_7P$	$[M-H_2O+H]^+$	714.5796	3.7	x
			$[M+H]^+$	732.5902	3.5	x
PE (36:1p)		$C_{41}H_{80}NO_7P$	$[M+Na+K-H]^+$	790.5124	0.2	x
PE (36:2p)	P-16:0, 20:2, P-18:1, 18:1	$C_{41}H_{78}NO_7P$	$[M+2K-H]^+$	804.4706	2.5	x
PE (36:3p)		$C_{41}H_{76}NO_7P$	$[M+Na+K-H]^+$	786.4811	1.3	x
PE (36:4p)		$C_{41}H_{74}NO_7P$	$[M+Na+K-H]^+$	784.4654	1.9	−3.2
			$[M+2K-H]^+$	800.4393	1	−2.8
PE (38:2p)		$C_{43}H_{82}NO_7P$	$[M+2K-H]^+$	832.5019	−2.4	x
PE (38:4p)		$C_{43}H_{78}NO_7P$	$[M+Na+K-H]^+$	812.4967	2.5	4.6
PE (38:5p)		$C_{43}H_{76}NO_7P$	$[M+K]^+$	788.4991	−0.9	x
			$[M+Na+K-H]^+$	810.4811	3.7	x
			$[M+2K-H]^+$	826.4550	3.9	x
PE (38:6p)		$C_{43}H_{74}NO_7P$	$[M+Na]^+$	770.5095	x	−1
			$[M+Na+K-H]^+$	808.4654	x	−0.5
			$[M+2K-H]^+$	824.4393	1.1	−0.9
PE (40:4p)		$C_{45}H_{82}NO_7P$	$[M+K]^+$	818.5461	0.2	−1
			$[M+Na+K-H]^+$	840.5280	x	1.4
			$[M+2K-H]^+$	856.5019	−2.7	1.6
PE (40:5p)		$C_{45}H_{80}NO_7P$	$[M+K]^+$	816.5304	0.1	x
			$[M+2K-H]^+$	854.4863	−0.7	x
PE (40:6p)	P-18:0, 22:6	$C_{45}H_{78}NO_7P$	$[M+K]^+$	814.5148	2.4	x
			$[M+2K-H]^+$	852.4706	−3.1	x
PE (42:7p)		C47H80NO7P	$[M+K]^+$	840.5304	−0.7	x
PE (42:8p)		$C_{47}H_{78}NO_7P$	$[M+H]^+$	800.5589	x	0.1
PE (30:1)		$C_{35}H_{68}NO_8P$	$[M+Na+K-H]^+$	722.4134	−2.1	x
PE (32:0)		$C_{37}H_{74}NO_8P$	$[M+K]^+$	730.4784	4.9	x
			$[M+2K-H]^+$	768.4343	4.6	x
PE (34:0)		$C_{39}H_{78}NO_8P$	$[M+2K-H]^+$	796.4656	4	4.1
PE (34:1)	16:0, 18:1	$C_{39}H_{76}NO_8P$	$[M+K]^+$	756.4940	3.2	x
			$[M+2K-H]^+$	794.4499	3.6	x
PE (34:5)		$C_{39}H_{68}NO_8P$	$[M+2K-H]^+$	786.3873	4.3	x
PE (36:0)		$C_{41}H_{82}NO_8P$	$[M-H_2O+H]^+$	730.5745	4.5	x
			$[M+H]^+$	748.5851	x	2.3
PE (36:1)		$C_{41}H_{80}NO_8P$	$[M+H]^+$	746.5694	x	3.7
			$[M+Na+K-H]^+$	806.5073	−1.7	x
			$[M+2K-H]^+$	822.4812	x	2.8
PE (36:2)	18:1, 18:1	$C_{41}H_{78}NO_8P$	$[M+2K-H]^+$	820.4656	3.4	3.3
PE (36:3)		$C_{41}H_{76}NO_8P$	$[M+K]^+$	780.4940	0.6	−0.2
PE (36:4)	16:0, 20:4	$C_{41}H_{74}NO_8P$	$[M+2K-H]^+$	816.4343	3.1	4.5
PE (38:1)		$C_{43}H_{84}NO_8P$	$[M+H]^+$	774.6007	x	1.5
			$[M+Na+K-H]^+$	834.5386	x	0.5
			$[M+2K-H]^+$	850.5125	−1.3	2.5
PE (38:2)	18:1, 20:1	$C_{43}H_{82}NO_8P$	$[M+2K-H]^+$	848.4969	1.7	x
PE (38:4)	18:0, 20:4	$C_{43}H_{78}NO_8P$	$[M+K]^+$	806.5097	x	0.9
			$[M+2K-H]^+$	844.4656	2.8	2.6
PE (38:6)	18:2, 20:4	$C_{43}H_{74}NO_8P$	$[M+H]^+$	764.5225	x	2.8
			$[M+K]^+$	802.4784	−1.4	2.1
			$[M+2K-H]^+$	840.4343	2.7	2.3

TABLE 1 (Continued)

Compound identification	Fatty acids from LC-MSMS	Chemical formula	Ionic species	Calc. m/z	NAPA Δm (ppm)	MALDI Δm (ppm)
PE (38:7)		$C_{43}H_{72}NO_8P$	$[M-H_2O+H]^+$	744.4963	x	−0.5
PE (40:1)		$C_{45}H_{88}NO_8P$	$[M+H]^+$	802.6320	x	1.9
			$[M+Na]^+$	824.6140	−2.5	x
PE (40:2)		$C_{45}H_{86}NO_8P$	$[M+H]^+$	800.6164	x	1.6
PE (40:4)	18:0, 22:4	$C_{45}H_{82}NO_8P$	$[M+H]^+$	796.5851	x	−0.5
			$[M+2K-H]^+$	872.4969	2.5	4.5
PE (40:6)	18:0, 22:6	$C_{45}H_{78}NO_8P$	$[M+K]^+$	830.5097	4.1	3.5
			$[M+2K-H]^+$	868.4656	1.5	2.5
PE (40:7)	18:1, 22:6	$C_{45}H_{76}NO_8P$	$[M-H_2O+H]^+$	772.5276	−0.3	−1.1
			$[M+K]^+$	828.4940	x	1
			$[M+2K-H]^+$	866.4499	2.1	2.2
PE (42:4)		$C_{47}H_{86}NO_8P$	$[M+2K-H]^+$	900.5282	−0.5	x
PE (42:6)		$C_{47}H_{82}NO_8P$	$[M+2K-H]^+$	896.4969	4	x
PE (42:7)		$C_{47}H_{80}NO_8P$	$[M+2Na-H]^+$	862.5333	−3.7	x
			$[M+2K-H]^+$	894.4812	3.1	x
PE (42:8)		$C_{47}H_{78}NO_8P$	$[M-H_2O+H]^+$	798.5432	−0.4	−0.9
			$[M+2Na-H]^+$	860.5177	−3.2	x
PG (36:1)		$C_{42}H_{81}O_{10}P$	$[M+K]^+$	815.5199	x	−1.2
PG (38:3)		$C_{44}H_{81}O_{10}P$	$[M+H]^+$	801.5640	2.4	x
			$[M+K]^+$	839.5199	1.8	x
PG (38:7)		$C_{44}H_{73}O_{10}P$	$[M+H]^+$	793.5014	−0.2	x
PG (40:5)		$C_{46}H_{81}O_{10}P$	$[M+Na+K-H]^+$	885.5018	2	x
PG (40:9)		$C_{46}H_{73}O_{10}P$	$[M+Na+K-H]^+$	877.4392	x	0.4
PG (42:10)		$C_{48}H_{75}O_{10}P$	$[M-H_2O+H]^+$	825.5065	4.9	x
PG (42:11)		$C_{48}H_{73}O_{10}P$	$[M+2K-H]^+$	917.4132	x	−2.8
PI (38:4)		$C_{47}H_{83}O_{13}P$	$[M+K]^+$	925.5203	0.7	2.4
			$[M+2Na-H]^+$	931.5283	x	0.2
			$[M+Na+K-H]^+$	947.5022	3.3	2.3
			$[M+2K-H]^+$	963.4762	2.7	2.6
PI (38:5)		$C_{47}H_{81}O_{13}P$	$[M+2K-H]^+$	961.4605	4.7	4.3
PI (40:4)		$C_{49}H_{87}O_{13}P$	$[M+2K-H]^+$	991.5075	x	2.9
PS (34:2)		$C_{40}H_{74}NO_{10}P$	$[M+2Na-H]^+$	804.4762	x	−2.8
PS (36:2)	18:1, 18:1	$C_{42}H_{78}NO_{10}P$	$[M+2Na-H]^+$	832.5075	x	−0.8
			$[M+2K-H]^+$	864.4554	1.5	x
PS (36:4)		$C_{42}H_{74}NO_{10}P$	$[M-H_2O+H]^+$	766.5017	4.8	x
PS (36:6)		$C_{42}H_{70}NO_{10}P$	$[M-H_2O+H]^+$	762.4705	1.5	x
PS (38:2)		$C_{44}H_{82}NO_{10}P$	$[M+Na+K-H]^+$	876.5127	−4.7	x
			$[M+2K-H]^+$	892.4867	−2.2	x
PS (38:4)	18:0, 20:4	$C_{44}H_{78}NO_{10}P$	$[M+2K-H]^+$	888.4554	x	1
PS (40:6)	18:0, 22:6	$C_{46}H_{78}NO_{10}P$	$[M+Na]^+$	858.5256	x	−0.5
			$[M+K]^+$	874.4995	x	3.2
			$[M+Na+K-H]^+$	896.4814	x	2.7
			$[M+2K-H]^+$	912.4554	−1.4	3.2
PS (42:7)		$C_{48}H_{80}NO_{10}P$	$[M+2K-H]^+$	938.4710	x	−1.2
PS (44:12)	22:6, 22:6	$C_{50}H_{74}NO_{10}P$	$[M+K]^+$	918.4682	1.8	−4
			$[M+Na+K-H]^+$	940.4501	−3.8	x
PS (44:7)		$C_{50}H_{84}NO_{10}P$	$[M+K]^+$	928.5465	4.1	x
Pyroglutamate		$C_5H_7NO_3$	$[M+2K-H]^+$	205.9616	−1.5	1.6
SM (d34:1)		$C_{39}H_{79}N_2O_6P$	$[M+Na]^+$	725.5568	x	1.2
SM (d36:1)		$C_{41}H_{83}N_2O_6P$	$[M+H]^+$	731.6062	x	2.3
			$[M+Na]^+$	753.5881	1.1	x
			$[M+K]^+$	769.5620	−4.4	2.2

TABLE 1 (Continued)

Compound identification	Fatty acids from LC-MSMS	Chemical formula	Ionic species	Calc. m/z	NAPA Δm (ppm)	MALDI Δm (ppm)
SM (d36:2)		$C_{41}H_{81}N_2O_6P$	$[M+K]^+$	767.5464	x	−1.8
SM (d38:1)		$C_{43}H_{87}N_2O_6P$	$[M+Na]^+$	781.6194	x	1.9
			$[M+K]^+$	797.5933	x	−1
SM (d38:4)		$C_{43}H_{81}N_2O_6P$	$[M+H]^+$	753.5905	x	−1.3
SM (d40:1)		$C_{45}H_{91}N_2O_6P$	$[M+Na]^+$	809.6507	x	2.7
			$[M+K]^+$	825.6246	x	2.6
TG (40:1)		$C_{43}H_{80}O_6$	$[M+Na+K-H]^+$	753.5406	0	x
TG (42:1)		$C_{45}H_{84}O_6$	$[M+2K-H]^+$	797.5458	4.3	x
TG (42:2)		$C_{45}H_{82}O_6$	$[M+Na+K-H]^+$	779.5562	x	5
TG (50:3)		$C_{53}H_{96}O_6$	$[M+H]^+$	829.7280	x	−1.1
TG (52:2)		$C_{55}H_{102}O_6$	$[M+K]^+$	897.7308	1.3	x
Tryptophan		$C_{11}H_{12}N_2O_2$	$[M+H]^+$	205.0972	x	4.5
			$[M+Na]^+$	227.0791	x	−0.1
Tyrosine		$C_9H_{11}NO_3$	$[M+H]^+$	182.0812	x	−4.5

TABLE 2 Metabolite and lipid assignments based on accurate mass (≤5 ppm mass error) for negative ion mode MSI analysis of mouse brain sections. Acyl chain compositions are reported for lipids identified in parallel by LC-MS/MS analysis

Compound identification	Fatty acids from LC-MSMS	Chemical formula	Ionic species	Calc. m/z	NAPA Δm (ppm)	MALDI Δm (ppm)
ADP		$C_{10}H_{15}N_5O_{10}P_2$	[M-H-H₂O]-	408.0116	x	1.2
			[M-H]-	426.0221	x	0.8
			[M-2H+Na]-	448.0041	x	1.6
			[M-2H+K]-	463.9780	x	1.8
ATP		$C_{10}H_{16}N_5O_{13}P_3$	[M-H-H₂O]-	487.9779	x	3.2
			[M-H]-	505.9885	x	2.4
			[M-2H+Na]-	527.9704	x	1.4
Carnitine (18:0)		$C_{25}H_{49}NO_4$	[M-2H+K]-	464.3148	1.3	1.8
CE (18:1)		$C_{45}H_{78}O_2$	[M-2H+K]-	687.5488	x	−4.6
CE (20:1)		$C_{47}H_{82}O_2$	[M+K-2H]-	715.5801	−4.2	−3.8
Cer (36:1)		$C_{36}H_{71}NO_3$	[M-H]-	564.5361	x	3.2
Cer (d40:2)		$C_{40}H_{77}NO_3$	[M-H]-	618.5831	1	x
Cer (d42:2)		$C_{42}H_{81}NO_3$	[M-H]-	646.6144	1	x
FA (12:0)		$C_{12}H_{24}O_2$	[M-H]-	199.1704	x	−4.3
FA (14:0)		$C_{14}H_{28}O_2$	[M-H]-	227.2017	x	−4.3
FA (15:0)		$C_{15}H_{30}O_2$	[M-H]-	241.2173	x	−2
FA (16:0)		$C_{16}H_{32}O_2$	[M-H]-	255.2330	−0.8	−1.3
FA (16:1)		$C_{16}H_{30}O_2$	[M-H]-	253.2173	x	−4.1
FA (18:0)		$C_{18}H_{36}O_2$	[M-H-H₂O]-	265.2537	x	0.4
			[M-H]-	283.2643	−3.8	0
FA (18:1)		$C_{18}H_{34}O_2$	[M-H]-	281.2486	−3.6	−3.1
			[M-2H+Na]-	303.2306	x	−2.2
FA (18:2)		$C_{18}H_{32}O_2$	[M-H]-	279.2330	x	0.6
FA (20:4)		$C_{20}H_{32}O_2$	[M-H]-	303.2330	−3.5	−3.6
FA (22:6)		$C_{22}H_{32}O_2$	[M-H]-	327.2330	−2.4	−0.6
FMN		$C_{17}H_{21}N_4O_9P$	[M-2H+K]-	493.0532	x	0.7
HexCer (d42:1)		$C_{48}H_{93}NO_8$	[M-H]-	810.6828	−2.1	x
HexCer (d42:2)		$C_{48}H_{91}NO_8$	[M-H]-	808.6672	−0.5	x
HexCer (d41:1)		$C_{47}H_{91}NO_8$	[M+K-2H]-	834.6231	3.9	x
HexCer (d42:1[2OH])		$C_{48}H_{93}NO_9$	[M-H]-	826.6778	−0.5	x
HexCer (d38:1[2OH])		$C_{44}H_{85}NO_9$	[M-H]-	770.6152	−1	x

TABLE 2   (Continued)

Compound identification	Fatty acids from LC-MSMS	Chemical formula	Ionic species	Calc. m/z	NAPA Δm (ppm)	MALDI Δm (ppm)
HexCer (d38:2[2OH])		$C_{44}H_{83}NO_9$	[M+K-2H-H$_2$O]-	788.5448	x	2
HexCer (d40:2[2OH])		$C_{46}H_{87}NO_9$	[M+K-2H-H$_2$O]-	816.5761	x	0.3
HexCer (t42:1[2OH])		$C_{48}H_{93}NO_{10}$	[M-H-H$_2$O]-	824.6621	−0.4	x
HexCer (t38:1[2OH])		$C_{44}H_{85}NO_{10}$	[M+K-2H]-	824.5660	x	−3.9
Glutamine		$C_5H_{10}N_2O_3$	[M-2H+K]-	183.0178	x	4.9
HexCer (t40:1)		$C_{46}H_{89}NO_9$	[M-H]-	798.6465	−0.4	x
Hexose-bisphosphate		$C_6H_{14}O_{12}P_2$	[M-H-H$_2$O]-	320.9782	x	−0.6
			[M-H]-	338.9888	x	2.4
			[M-2H+Na]-	360.9707	x	0.1
			[M-2H+K]-	376.9447	x	0.8
Hexose-phosphate		$C_6H_{13}O_9P$	[M-H-H$_2$O]-	241.0119	x	−1.1
			[M-H]-	259.0224	x	−4.9
LysoPC (22:4)		$C_{30}H_{54}NO_7P$	[M-2H+K]-	608.3124	x	0.4
LysoPE (16:0)		$C_{21}H_{44}NO_7P$	[M-H]-	452.2783	x	0.7
LysoPE (18:0)		$C_{23}H_{48}NO_7P$	[M-H-H$_2$O]-	462.2990	1.1	1.7
			[M-H]-	480.3096	1.6	2.2
			[M-2H+Na]-	502.2915	1.8	x
LysoPE (18:1)		$C_{23}H_{46}NO_7P$	[M-H]-	478.2939	x	1.8
LysoPE (20:1)		$C_{25}H_{50}NO_7P$	[M-H]-	506.3252	x	1.5
LysoPE (20:2)		$C_{25}H_{48}NO_7P$	[M-H-H$_2$O]-	486.2990	−2.8	x
LysoPE (22:4)		$C_{27}H_{48}NO_7P$	[M-2H+K]-	566.2655	x	0.9
LysoPE (22:6)		$C_{27}H_{44}NO_7P$	[M-H-H$_2$O]-	506.2677	4.4	x
			[M-H]-	524.2783	3.6	x
			[M-2H+Na]-	546.2602	3.4	x
LysoPI (18:0)		$C_{27}H_{53}O_{12}P$	[M-H-H$_2$O]-	581.3096	x	3.2
			[M-H]-	599.3202	x	2.6
LysoPI (18:1)		$C_{27}H_{51}O_{12}P$	[M-H-H$_2$O]-	579.2940	x	2.7
			[M-H]-	597.3045	x	2.5
LysoPI (20:4)		$C_{29}H_{49}O_{12}P$	[M-H-H$_2$O]-	601.2783	x	3.4
			[M-H]-	619.2889	x	2.8
LysoPS (18:0)		$C_{24}H_{48}NO_9P$	[M-H-H$_2$O]-	506.2888	x	2.4
			[M-2H+Na]-	546.2813	x	2.8
PA (32:0)		$C_{35}H_{69}O_8P$	[M-H]-	647.4657	x	1.6
PA (34:1)		$C_{37}H_{71}O_8P$	[M-H]-	673.4814	1.5	2.2
PA (36:1)		$C_{39}H_{75}O_8P$	[M-H]-	701.5127	x	2
PA (36:2)		$C_{39}H_{73}O_8P$	[M-H]-	699.4970	0.8	2.2
PA (38:1)		$C_{41}H_{79}O_8P$	[M-H]-	729.5440	x	2.6
PA (38:3)		$C_{41}H_{75}O_8P$	[M-H]-	725.5127	3	x
			[M-2H+K]-	763.4686	x	1.1
PA (38:4)		$C_{41}H_{73}O_8P$	[M-H]-	723.4970	4.4	2
PA (38:5)		$C_{41}H_{71}O_8P$	[M-H]-	721.4814	1.4	2.1
PA (38:6)		$C_{41}H_{69}O_8P$	[M-H]-	719.4657	x	1
PA (40:1)		$C_{43}H_{83}O_8P$	[M-2H+K]-	795.5312	x	0
PA (40:5)		$C_{43}H_{75}O_8P$	[M-H-H$_2$O]-	731.5021	x	3
PA (40:6)		$C_{43}H_{73}O_8P$	[M-H]-	747.4970	x	1
PA (40:7)		$C_{43}H_{71}O_8P$	[M-H]-	745.4814	1.1	1
PA (42:2)		$C_{45}H_{85}O_8P$	[M-2H+K]-	821.5468	x	0.1
PA (42:7)		$C_{45}H_{75}O_8P$	[M-H]-	773.5127	1.7	x
PA (42:8)		$C_{45}H_{73}O_8P$	[M-2H+K]-	809.4529	x	1.8
PA (44:2)		$C_{47}H_{89}O_8P$	[M-2H+K]-	849.5781	x	−0.3

TABLE 2 (Continued)

Compound identification	Fatty acids from LC-MSMS	Chemical formula	Ionic species	Calc. m/z	NAPA Δm (ppm)	MALDI Δm (ppm)
PC (32:3)		$C_{40}H_{74}NO_8P$	[M-2H+K]-	764.4638	x	0.8
PC (34:3)		$C_{42}H_{78}NO_8P$	[M-2H+K]-	792.4951	x	−0.9
PC (36:2)	18:0, 18:2, 18:1, 18:1	$C_{44}H_{84}NO_8P$	[M-2H+K]-	822.5421	x	1.4
PC (38:0)		$C_{46}H_{92}NO_8P$	[M-2H+K]-	854.6047	x	4
PC (38:1)	18:0, 20:1	$C_{46}H_{90}NO_8P$	[M-2H+K]-	852.5890	x	3.1
PC (38:2)	18:1, 20:1	$C_{46}H_{88}NO_8P$	[M-2H+K]-	850.5734	x	0.1
PC (40:2)		$C_{48}H_{92}NO_8P$	[M-2H+K]-	878.6047	−2.9	0.4
PC (42:2)	18:1, 24:1	$C_{50}H_{96}NO_8P$	[M-2H+K]-	906.6360	−1.8	−1
PC (42:3)		$C_{50}H_{94}NO_8P$	[M-2H+K]-	904.6203	−2	−1.1
PC (44:2)		$C_{52}H_{100}NO_8P$	[M-2H+K]-	934.6673	x	−3.7
PE (34:1p)	P-16:0, 18:1, P-18:1, 16:0	$C_{39}H_{76}NO_7P$	[M-H]-	700.5287	−3.6	x
PE (36:1p)	P-16:0, 20:1, P-18:0, 18:1	$C_{41}H_{80}NO_7P$	[M-H]-	728.5600	0.1	0.6
PE (36:2p)	P-18:1, 18:1	$C_{41}H_{78}NO_7P$	[M-H]-	726.5443	0.1	2.2
PE (36:3p)	P-16:0, 20:3	$C_{41}H_{76}NO_7P$	[M-H]-	724.5287	−2.2	x
			[M+Na-2H]-	746.5106	x	−3.5
PE (36:4p)	P-16:0, 20:4	$C_{41}H_{74}NO_7P$	[M-H]-	722.5130	−1.1	x
PE (38:2p)	P-18:1, 20:1, P-20:1, 18:1	$C_{43}H_{82}NO_7P$	[M-H]-	754.5756	−0.2	0.8
PE (38:4p)	P-16:0, 22:4, P-18:0, 20:4	$C_{43}H_{78}NO_7P$	[M-H]-	750.5443	0.2	x
PE (38:5p)	P-18:1, 20:4	$C_{43}H_{76}NO_7P$	[M-H]-	748.5287	−0.8	x
PE (38:6p)	P-16:0, 22:6	$C_{43}H_{74}NO_7P$	[M-H]-	746.5130	−0.3	x
			[M+Na-2H-H_2O]-	750.4844	x	0
PE (40:4p)	P-18:0, 22:4, P-18:0, 22:4	$C_{45}H_{82}NO_7P$	[M-H]-	778.5756	0.9	x
PE (40:6p)	P-18:0, 22:6	$C_{45}H_{78}NO_7P$	[M-H]-	774.5443	0	0.9
PE (42:6p)		$C_{47}H_{82}NO_7P$	[M+Na-2H-H_2O]-	806.5470	x	−0.4
PE (42:8p)		$C_{47}H_{78}NO_7P$	[M+Na-2H-H_2O]-	802.5157	x	2.7
PE (34:0)		$C_{39}H_{78}NO_8P$	[M-H]-	718.5392	1.5	1.5
PE (34:1)	16:0, 18:1	$C_{39}H_{76}NO_8P$	[M-H]-	716.5236	0.9	2.3
PE (36:1)	16:0, 20:1, 18:0, 18:1	$C_{41}H_{80}NO_8P$	[M-H]-	744.5549	0.4	1.4
PE (36:2)	18:1, 18:1	$C_{41}H_{78}NO_8P$	[M-H]-	742.5392	0.2	1.6
PE (36:3)		$C_{41}H_{76}NO_8P$	[M-2H+K]-	778.4795	x	−0.6
PE (36:4)	16:0, 20:4	$C_{41}H_{74}NO_8P$	[M-H]-	738.5079	1	x
PE (38:0)		$C_{43}H_{86}NO_8P$	[M-H-H_2O]-	756.5913	0.3	0.4
PE (38:1)		$C_{43}H_{84}NO_8P$	[M-H]-	772.5862	0.3	0.9
PE (38:2)	18:1, 20:1	$C_{43}H_{82}NO_8P$	[M-H]-	770.5705	0.6	1.2
PE (38:4)	18:0, 20:4	$C_{43}H_{78}NO_8P$	[M-H]-	766.5392	0.5	1.2
PE (38:5)	16:0, 22:5, 18:1, 20:4	$C_{43}H_{76}NO_8P$	[M-H]-	764.5236	0.2	−3.1
PE (38:6)	16:0, 22:6	$C_{43}H_{74}NO_8P$	[M-H]-	762.5079	0.5	−2.9
PE (40:1)		$C_{45}H_{88}NO_8P$	[M-H-H_2O]-	782.6069	−0.4	x
PE (40:4)	18:0, 22:4	$C_{45}H_{82}NO_8P$	[M-H-H_2O]-	776.5600	−1.1	x
			[M-H]-	794.5705	1.5	x
PE (40:6)	18:0, 22:6	$C_{45}H_{78}NO_8P$	[M-H-H_2O]-	772.5287	0.3	x
			[M-H]-	790.5392	0	0.5
PE (40:7)	18:1, 22:6	$C_{45}H_{76}NO_8P$	[M-H]-	788.5236	0.5	x
PE (40:9)		$C_{45}H_{72}NO_8P$	[M-H-H_2O]-	766.4817	x	−3
PE (42:6)		$C_{47}H_{82}NO_8P$	[M-H]-	818.5705	1.3	x

TABLE 2 (Continued)

Compound identification	Fatty acids from LC-MSMS	Chemical formula	Ionic species	Calc. m/z	NAPA Δm (ppm)	MALDI Δm (ppm)
PE (44:2)		$C_{49}H_{94}NO_8P$	[M-2H+K]-	892.6203	3.2	−1.5
PG (38:6)		$C_{44}H_{75}O_{10}P$	[M-2H+K]-	831.4584	x	−3.7
PG (40:8)		$C_{46}H_{75}O_{10}P$	[M-2H+K]-	855.4584	x	−0.8
PG (44:12)		$C_{50}H_{75}O_{10}P$	[M-2H+K]-	903.4584	x	−1.5
PI (32:0)		$C_{41}H_{79}O_{13}P$	[M-H]-	809.5186	x	−4.1
PI (34:0)		$C_{43}H_{83}O_{13}P$	[M-H]-	837.5499	x	−4.1
PI (34:1)		$C_{43}H_{81}O_{13}P$	[M-H]-	835.5342	x	−2.9
PI (36:4)	16:0, 20:4	$C_{45}H_{79}O_{13}P$	[M-H]-	857.5186	x	0.7
PI (38:4)	18:0, 20:4	$C_{47}H_{83}O_{13}P$	[M-H]-	885.5499	0	1
PI (38:5)		$C_{47}H_{81}O_{13}P$	[M-H]-	883.5342	x	1.4
PI (38:6)	16:0, 22:6	$C_{47}H_{79}O_{13}P$	[M-H]-	881.5186	x	2
PI (40:6)	18:0, 22:6	$C_{49}H_{83}O_{13}P$	[M-H]-	909.5499	x	1.4
PS (36:2)	18:1, 18:1	$C_{42}H_{78}NO_{10}P$	[M-H]-	786.5291	x	2.3
PS (38:4)	18:0, 20:4	$C_{44}H_{78}NO_{10}P$	[M-H]-	810.5291	x	0.4
PS (40:6)	18:0, 22:6	$C_{46}H_{78}NO_{10}P$	[M-2H+Na]-	856.5110	x	0.7
ST (d30:2)		$C_{36}H_{67}NO_{11}S$	[M-H]-	720.4362	x	1.9
ST (d36:1)		$C_{42}H_{81}NO_{11}S$	[M-H]-	806.5458	−0.1	x
ST (d36:2)		$C_{42}H_{79}NO_{11}S$	[M-H]-	804.5301	x	−4.3
ST (d38:1)		$C_{44}H_{85}NO_{11}S$	[M-H]-	834.5771	x	1.4
ST (d38:2)		$C_{44}H_{83}NO_{11}S$	[M-H]-	832.5614	x	1.5
ST (d40:1)		$C_{46}H_{89}NO_{11}S$	[M-H]-	862.6084	0.1	1.6
ST (d40:2)		$C_{46}H_{87}NO_{11}S$	[M-H]-	860.5927	x	1.9
ST (d40:3)		$C_{46}H_{85}NO_{11}S$	[M-H]-	858.5771	x	2.8
ST (d42:1)		$C_{48}H_{93}NO_{11}S$	[M-H-H$_2$O]-	872.6291	x	−0.5
			[M-H]-	890.6397	−0.7	0.2
ST (d42:2)		$C_{48}H_{91}NO_{11}S$	[M-H-H$_2$O]-	870.6134	x	2.8
			[M-H]-	888.6240	−0.5	x
ST (d42:3)		$C_{48}H_{89}NO_{11}S$	[M-H]-	886.6084	x	1.6
ST (d44:2)		$C_{50}H_{95}NO_{11}S$	[M-H]-	916.6553	x	−4.6
Tyrosine		$C_9H_{11}NO_3$	[M-2H+Na]-	202.0486	x	0.9
UDP-glucuronate		$C_{15}H_{22}N_2O_{18}P_2$	[M-H]-	579.0270	x	2.4

enters the plume with significant amounts of matrix material. The acidic (e.g., DHB) or basic (e.g., 9-AA) matrix facilitates proton exchange to generate ions from desorbed analyte molecules.

In NAPA-LDI-MSI, the tissue section to be analyzed is placed on top of the NAPA. During analysis, the laser radiation penetrates through the tissue and is absorbed by the underlying nanoposts. Rapid heating of the nanoposts causes volatilization of a significant amount of the deposited material, and the plume is composed primarily of this ejected sample. The reduced availability of proton donors and increased availability of alkali metal cations (Na$^+$ and K$^+$) from the desorbed tissue favors generation of metal adduct ions and the detection of species which form stable alkali metal adducts. This hypothesis is consistent with the predominance of alkali metal adduct ions in the positive mode NAPA data found in Table 1.

5 | CONCLUSIONS

Our results show that NAPA-LDI-MSI offers enhanced ionization of certain lipid classes including PE, PEp, and HexCer that are difficult to

detect using traditional MALDI matrices and have important roles in signaling and disease. Furthermore, given the uniformity of the nano-fabricated NAPA imaging chips, this platform offers the possibility to perform higher resolution imaging without specialized matrix deposition for MSI of biological tissues. Other studies also indicate broader dynamic range for quantitation by NAPA-LDI-MS compared to MALDI-MS. This indicates the potential of the nanofabricated platform for quantitative imaging, a longstanding goal in MSI. The complementarity of lipid coverage between NAPA-LDI-MSI and MALDI-MSI offers the potential for selective analysis of lipid species of interest. Applied in parallel, these complementary MSI platforms allow for significantly broader coverage of lipid classes, extending the capabilities of MSI for lipidomics in brain tissues.

authors and should not be interpreted as representing the official policies, either expressed or implied, of the Army Research Office, DARPA, or the U.S. Government. The U.S. Government is authorized to reproduce and distribute reprints for Government purposes notwithstanding any copyright notation hereon.

CONFLICT OF INTEREST

The authors declare that they have no conflict of interest to declare.

AUTHORS CONTRIBUTIONS

A.V., J.A.F., and J.E.D. conceived the study, and J.A.F., J.E.D., and A.R.K. conducted the experiments. J.A.F., J.E.D., A.R.K., and A.V. performed the data analysis. N.J.M performed the nanofabrication of the NAPA substrates. S.Y. performed the mouse brain dissections. J.A.F., A.R.K, and A.V. wrote the manuscript.

ORCID

Jarod A. Fincher https://orcid.org/0000-0002-1717-3368
Akos Vertes https://orcid.org/0000-0001-5186-5352

REFERENCES

Alexandrov, T. (2012). MALDI imaging mass spectrometry: Statistical data analysis and current computational challenges. *BMC Bioinformatics*, *13*, 1–13. https://doi.org/10.1186/1471-2105-13-s16-s11

Baluya, D. L., Garrett, T. J., & Yost, R. A. (2007). Automated MALDI matrix deposition method with inkjet printing for imaging mass spectrometry. *Analytical Chemistry*, *79*(17), 6862–6867. https://doi.org/10.1021/ac070958d

Braidy, N., Poljak, A., Marjo, C., Rutlidge, H., Rich, A., Jayasena, T., … Sachdev, P. (2014). Metal and complementary molecular bioimaging in Alzheimer's disease. *Frontiers in Aging Neuroscience*, *6*. https://doi.org/10.3389/fnagi.2014.00138

Buchberger, A. R., DeLaney, K., Johnson, J., & Li, L. J. (2018). Mass spectrometry imaging: A review of emerging advancements and future insights. *Analytical Chemistry*, *90*(1), 240–265. https://doi.org/10.1021/acs.analchem.7b04733

Burnum, K. E., Cornett, D. S., Puolitaival, S. M., Milne, S. B., Myers, D. S., Tranguch, S., … Caprioli, R. M. (2009). Spatial and temporal alterations of phospholipids determined by mass spectrometry during mouse embryo implantation. *Journal of Lipid Research*, *50*(11), 2290–2298. https://doi.org/10.1194/jlr.M900100-JLR200

Caprioli, R. M., Farmer, T. B., & Gile, J. (1997). Molecular imaging of biological samples: Localization of peptides and proteins using MALDI-TOF MS. *Analytical Chemistry*, *69*(23), 4751–4760. https://doi.org/10.1021/ac970888i

Chan, R. B., Oliveira, T. G., Cortes, E. P., Honig, L. S., Duff, K. E., Small, S. A., … Di Paolo, G. (2012). Comparative lipidomic analysis of mouse and human brain with Alzheimer disease. *Journal of Biological Chemistry*, *287*(4), 2678–2688. https://doi.org/10.1074/jbc.M111.274142

Colsch, B., & Woods, A. S. (2010). Localization and imaging of sialylated glycosphingolipids in brain tissue sections by MALDI mass spectrometry. *Glycobiology*, *20*(6), 661–667. https://doi.org/10.1093/glycob/cwq031

Di Paolo, G., & Kim, T. W. (2011). Linking lipids to Alzheimer's disease: Cholesterol and beyond. *Nature Reviews Neuroscience*, *12*(5), 284–296. https://doi.org/10.1038/nrn3012

Goodwin, R. J. A. (2012). Sample preparation for mass spectrometry imaging: Small mistakes can lead to big consequences. *Journal of Proteomics*, *75*(16), 4893–4911. https://doi.org/10.1016/j.jprot.2012.04.012

Gowda, G. A. N., Zhang, S. C., Gu, H. W., Asiago, V., Shanaiah, N., & Raftery, D. (2008). Metabolomics-based methods for early disease diagnostics. *Expert Review of Molecular Diagnostics*, *8*(5), 617–633. https://doi.org/10.1586/14737159.8.5.617

Greving, M. P., Patti, G. J., & Siuzdak, G. (2011). Nanostructure-initiator mass spectrometry metabolite analysis and imaging. *Analytical Chemistry*, *83*(1), 2–7. https://doi.org/10.1021/ac101565f

Grimm, M. O. W., Kuchenbecker, J., Rothhaar, T. L., Grosgen, S., Hundsdorfer, B., Burg, V. K., … Hartmann, T. (2011). Plasmalogen synthesis is regulated via alkyl-dihydroxyacetonephosphate-synthase by amyloid precursor protein processing and is affected in Alzheimer's disease. *Journal of Neurochemistry*, *116*(5), 916–925. https://doi.org/10.1111/j.1471-4159.2010.07070.x

Hong, J. H., Kang, J. W., Kim, D. K., Baik, S. H., Kim, K. H., Shanta, S. R., … Kim, K. P. (2016). Global changes of phospholipids identified by MALDI imaging mass spectrometry in a mouse model of Alzheimer's disease. *Journal of Lipid Research*, *57*(1), 36–45. https://doi.org/10.1194/jlr.M057869

Hutchinson, R. W., Cox, A. G., McLeod, C. W., Marshall, P. S., Harper, A., Dawson, E. L., & Howlett, D. R. (2005). Imaging and spatial distribution of beta-amyloid peptide and metal ions in Alzheimer's plaques by laser ablation-inductively coupled plasma-mass spectrometry. *Analytical Biochemistry*, *346*(2), 225–233. https://doi.org/10.1016/j.ab.2005.08.024

Jackson, S. N., Ugarov, M., Egan, T., Post, J. D., Langlais, D., Schultz, J. A., & Woods, A. S. (2007). MALDI-ion mobility-TOFMS imaging of lipids in rat brain tissue. *Journal of Mass Spectrometry*, *42*(8), 1093–1098. https://doi.org/10.1002/jms.1245

Kertesz, V., Van Berkel, G. J., Vavrek, M., Koeplinger, K. A., Schneider, B. B., & Covey, T. R. (2008). Comparison of drug distribution images from whole-body thin tissue sections obtained using desorption electrospray ionization tandem mass spectrometry and autoradiography. *Analytical Chemistry*, *80*(13), 5168–5177. https://doi.org/10.1021/ac800546a

Khan, M., Singh, J., & Singh, I. (2008). Plasmalogen deficiency in cerebral adrenoleukodystrophy and its modulation by lovastatin. *Journal of Neurochemistry*, *106*(4), 1766–1779. https://doi.org/10.1111/j.1471-4159.2008.05513.x

Koelmel, J. P., Kroeger, N. M., Ulmer, C. Z., Bowden, J. A., Patterson, R. E., Cochran, J. A., … Yost, R. A. (2017). LipidMatch: An automated workflow for rule-based lipid identification using untargeted high-resolution tandem mass spectrometry data. *BMC Bioinformatics*, *18*, 331. https://doi.org/10.1186/s12859-017-1744-3

Korte, A. R., Stopka, S. A., Morris, N., Razungunzwa, T., & Vertes, A. (2016). Large-scale metabolite analysis of standards and human serum by laser desorption ionization mass spectrometry from silicon nanopost arrays. *Analytical Chemistry*, *88*(18), 8989–8996. https://doi.org/10.1021/acs.analchem.6b01186

Lee, S. T., Lee, J. C., Kim, J. W., Cho, S. Y., Seong, J. K., & Moon, M. H. (2016). Global changes in lipid profiles of mouse cortex, hippocampus, and hypothalamus upon p53 knockout. *Scientific Reports*, *6*, 36510. https://doi.org/10.1038/srep36510

Miura, D., Fujimura, Y., Yamato, M., Hyodo, F., Utsumi, H., Tachibana, H., & Wariishi, H. (2010). Ultrahighly sensitive in situ metabolomic imaging for visualizing spatiotemporal metabolic behaviors. *Analytical Chemistry*, *82*(23), 9789–9796. https://doi.org/10.1021/ac101998z

Morris, N. J., Anderson, H., Thibeault, B., Vertes, A., Powell, M. J., & Razungunzwa, T. T. (2015). Laser desorption ionization (LDI) silicon nanopost array chips fabricated using deep UV projection lithography and deep reactive ion etching. *RSC Advances*, *5*(88), 72051–72057. https://doi.org/10.1039/c5ra11875a

Murphy, R. C., Hankin, J. A., & Barkley, R. M. (2009). Imaging of lipid species by MALDI mass spectrometry. *Journal of Lipid Research*, *50*, S317–S322. https://doi.org/10.1194/jlr.R800051-JLR200

Nemes, P., & Vertes, A. (2007). Laser ablation electrospray ionization for atmospheric pressure, in vivo, and imaging mass spectrometry. *Analytical Chemistry*, *79*(21), 8098–8106. https://doi.org/10.1021/ac071181r

Nemes, P., Woods, A. S., & Vertes, A. (2010). Simultaneous imaging of small metabolites and lipids in rat brain tissues at atmospheric pressure by laser ablation electrospray ionization mass spectrometry. *Analytical Chemistry*, *82*(3), 982–988. https://doi.org/10.1021/ac902245p

Neubert, P., & Walch, A. (2013). Current frontiers in clinical research application of MALDI imaging mass spectrometry. *Expert Review of Proteomics*, 10(3), 259–273. https://doi.org/10.1586/epr.13.19

Northen, T. R., Yanes, O., Northen, M. T., Marrinucci, D., Uritboonthai, W., Apon, J., ... Siuzdak, G. (2007). Clathrate nanostructures for mass spectrometry. *Nature*, 449(7165), 1033–U1033. https://doi.org/10.1038/nature06195

Potocnik, N. O., Porta, T., Becker, M., Heeren, R. M. A., & Ellis, S. R. (2015). Use of advantageous, volatile matrices enabled by next-generation high-speed matrix-assisted laser desorption/ionization time-of-flight imaging employing a scanning laser beam. *Rapid Communications in Mass Spectrometry*, 29(23), 2195–2203. https://doi.org/10.1002/rcm.7379

Puolitaival, S. M., Burnum, K. E., Cornett, D. S., & Caprioli, R. M. (2008). Solvent-free matrix dry-coating for MALDI imaging of phospholipids. *Journal of the American Society for Mass Spectrometry*, 19(6), 882–886. https://doi.org/10.1016/j.jasms.2008.02.013

Roux, A., Muller, L., Jackson, S. N., Post, J., Baldwin, K., Hoffer, B., ... Woods, A. S. (2016). Mass spectrometry imaging of rat brain lipid profile changes over time following traumatic brain injury. *Journal of Neuroscience Methods*, 272, 19–32. https://doi.org/10.1016/j.jneumeth.2016.02.004

Schubert, K. O., Weiland, F., Baune, B. T., & Hoffmann, P. (2016). The use of MALDI-MSI in the investigation of psychiatric and neurodegenerative disorders: A review. *Proteomics*, 16(11–12), 1747–1758. https://doi.org/10.1002/pmic.201500460

Seeley, E. H., Oppenheimer, S. R., Mi, D., Chaurand, P., & Caprioli, R. M. (2008). Enhancement of protein sensitivity for MALDI imaging mass spectrometry after chemical treatment of tissue sections. *Journal of the American Society for Mass Spectrometry*, 19(8), 1069–1077. https://doi.org/10.1016/j.jasms.2008.03.016

Shariatgorji, M., Svenningsson, P., & Andren, P. E. (2014). Mass spectrometry imaging, an emerging technology in neuropsychopharmacology. *Neuropsychopharmacology*, 39(1), 34–49. https://doi.org/10.1038/npp.2013.215

Shen, Z. X., Thomas, J. J., Averbuj, C., Broo, K. M., Engelhard, M., Crowell, J. E., ... Siuzdak, G. (2001). Porous silicon as a versatile platform for laser desorption/ionization mass spectrometry. *Analytical Chemistry*, 73(3), 612–619. https://doi.org/10.1021/ac000746f

Sjovall, P., Lausmaa, J., & Johansson, B. (2004). Mass spectrometric imaging of lipids in brain tissue. *Analytical Chemistry*, 76(15), 4271–4278. https://doi.org/10.1021/ac049389p

Skraskova, K., Claude, E., Jones, E. A., Towers, M., Ellis, S. R., & Heeren, R. M. A. (2016). Enhanced capabilities for imaging gangliosides in murine brain with matrix-assisted laser desorption/ionization and desorption electrospray ionization mass spectrometry coupled to ion mobility separation. *Methods*, 104, 69–78. https://doi.org/10.1016/j.ymeth.2016.02.014

Stopka, S. A., Holmes, X. A., Korte, A. R., Compton, L. R., Retterer, S. T., & Vertes, A. (2018). Trace analysis and reaction monitoring by nanophotonic ionization mass spectrometry from elevated bowtie and silicon nanopost arrays. *Advanced Functional Materials*, 28, 1801730. https://doi.org/10.1002/adfm.201801730

Stopka, S. A., Rong, C., Korte, A. R., Yadavilli, S., Nazarian, J., Razunguzwa, T. T., ... Vertes, A. (2016). Molecular imaging of biological samples on nanophotonic laser desorption ionization platforms. *Angewandte Chemie-International Edition*, 55(14), 4482–4486. https://doi.org/10.1002/anie.201511691

Strohalm, M., Kavan, D., Novak, P., Volny, M., & Havlicek, V. (2010). mMass 3: A cross-platform software environment for precise analysis of mass spectrometric data. *Analytical Chemistry*, 82(11), 4648–4651. https://doi.org/10.1021/ac100818g

Takats, Z., Wiseman, J. M., Gologan, B., & Cooks, R. G. (2004). Mass spectrometry sampling under ambient conditions with desorption electrospray ionization. *Science*, 306(5695), 471–473. https://doi.org/10.1126/science.1104404

Thomas, A., Charbonneau, J. L., Fournaise, E., & Chaurand, P. (2012). Sublimation of new matrix candidates for high spatial resolution imaging mass spectrometry of lipids: Enhanced information in both positive and negative polarities after 1,5-Diaminonapthalene deposition. *Analytical Chemistry*, 84(4), 2048–2054. https://doi.org/10.1021/ac2033547

Todd, P. J., Schaaff, T. G., Chaurand, P., & Caprioli, R. M. (2001). Organic ion imaging of biological tissue with secondary ion mass spectrometry and matrix-assisted laser desorption/ionization. *Journal of Mass Spectrometry*, 36(4), 355–369. https://doi.org/10.1002/jms.153

Touboul, D., Halgand, F., Brunelle, A., Kersting, R., Tallarek, E., Hagenhoff, B., & Laprevote, O. (2004). Tissue molecular ion imaging by gold cluster ion bombardment. *Analytical Chemistry*, 76(6), 1550–1559. https://doi.org/10.1021/ac035243z

Walker, B. N., Stolee, J. A., Pickel, D. L., Retterer, S. T., & Vertes, A. (2010). Tailored silicon nanopost arrays for resonant nanophotonic ion production. *Journal of Physical Chemistry C*, 114(11), 4835–4840. https://doi.org/10.1021/jp9110103

Walker, B. N., Stolee, J. A., & Vertes, A. (2012). Nanophotonic ionization for ultratrace and single-cell analysis by mass spectrometry. *Analytical Chemistry*, 84(18), 7756–7762. https://doi.org/10.1021/ac301238k

Watanabe, K., Sato, K., Biernat, W., Tachibana, O., von Ammon, K., Ogata, N., ... Ohgaki, H. (1997). Incidence and timing of p53 mutations during astrocytoma progression in patients with multiple biopsies. *Clinical Cancer Research*, 3(4), 523–530.

Watanabe, K., Sato, K., Yonekawa, Y., Kleihues, P., & Ohgaki, H. (1996). Overexpression of the EGF receptor and p53 mutations are mutually exclusive in the evolution of primary and secondary glioblastomas. *Brain Pathology*, 6(3), 217–223. https://doi.org/10.1111/j.1750-3639.1996.tb00848.x

Wei, J., Buriak, J. M., & Siuzdak, G. (1999). Desorption-ionization mass spectrometry on porous silicon. *Nature*, 399(6733), 243–246. https://doi.org/10.1038/20400

Wiseman, J. M., Ifa, D. R., Song, Q. Y., & Cooks, R. G. (2006). Tissue imaging at atmospheric pressure using desorption electrospray ionization (DESI) mass spectrometry. *Angewandte Chemie-International Edition*, 45(43), 7188–7192. https://doi.org/10.1002/anie.200602449

Woods, A. S., Colsch, B., Jackson, S. N., Post, J., Baldwin, K., Roux, A., ... Balaban, C. (2013). Gangliosides and ceramides change in a mouse model of blast induced traumatic brain injury. *ACS Chemical Neuroscience*, 4(4), 594–600. https://doi.org/10.1021/cn300216h

Wu, Q., Chu, J. L., Rubakhin, S. S., Gillette, M. U., & Sweedler, J. V. (2017). Dopamine-modified TiO_2 monolith-assisted LDI MS imaging for simultaneous localization of small metabolites and lipids in mouse brain tissue with enhanced detection selectivity and sensitivity. *Chemical Science*, 8(5), 3926–3938. https://doi.org/10.1039/c7sc00937b

Yanes, O., Woo, H. K., Northen, T. R., Oppenheimer, S. R., Shriver, L., Apon, J., ... Siuzdak, G. (2009). Nanostructure initiator mass spectrometry: Tissue imaging and direct biofluid analysis. *Analytical Chemistry*, 81(8), 2969–2975. https://doi.org/10.1021/ac802576q

Zavalin, A., Todd, E. M., Rawhouser, P. D., Yang, J. H., Norris, J. L., & Caprioli, R. M. (2012). Direct imaging of single cells and tissue at subcellular spatial resolution using transmission geometry MALDI MS. *Journal of Mass Spectrometry*, 47(11), 1473–1481. https://doi.org/10.1002/jms.3108